



HAL
open science

Entropy Engineering of 2D Materials

Hao Mei, Yuxuan Zhang, Panpan Zhang, Antonio Gaetano Ricciardulli, Paolo Samorì, Sheng Yang

► **To cite this version:**

Hao Mei, Yuxuan Zhang, Panpan Zhang, Antonio Gaetano Ricciardulli, Paolo Samorì, et al.. Entropy Engineering of 2D Materials. *Advanced Science*, 2024, 11 (46), pp.e2409404. 10.1002/advs.202409404 . hal-04835320

HAL Id: hal-04835320

<https://hal.science/hal-04835320v1>

Submitted on 13 Dec 2024

HAL is a multi-disciplinary open access archive for the deposit and dissemination of scientific research documents, whether they are published or not. The documents may come from teaching and research institutions in France or abroad, or from public or private research centers.

L'archive ouverte pluridisciplinaire **HAL**, est destinée au dépôt et à la diffusion de documents scientifiques de niveau recherche, publiés ou non, émanant des établissements d'enseignement et de recherche français ou étrangers, des laboratoires publics ou privés.



Distributed under a Creative Commons Attribution 4.0 International License

Entropy Engineering of 2D Materials

Hao Mei, Yuxuan Zhang, Panpan Zhang, Antonio Gaetano Ricciardulli,* Paolo Samori,* and Sheng Yang*

Entropy, a measure of disorder or uncertainty in the thermodynamics system, has been widely used to confer desirable functions to alloys and ceramics. The incorporation of three or more principal elements into a single sublattice increases the entropy to medium and high levels, imparting these materials a mélange of advanced mechanical and catalytic properties. In particular, when scaling down the dimensionality of crystals from bulk to the 2D space, the interplay between entropy stabilization and quantum confinement offers enticing opportunities for exploring new fundamental science and applications, since the structural ordering, phase stability, and local electronic states of these distorted 2D materials get significantly reshaped. During the last few years, the large family of high-entropy 2D materials is rapidly expanding to host MXenes, hydrotalcites, chalcogenides, metal-organic frameworks (MOFs), and many other uncharted members. Here, the recent advances in this dynamic field are reviewed, elucidating the influence of entropy on the fundamental properties and underlying elementary mechanisms of 2D materials. In particular, their structure-property relationships resulting from theoretical predictions and experimental findings are discussed. Furthermore, an outlook on the key challenges and opportunities of such an emerging field of 2D materials is also provided.

1. Introduction

In the course of human civilization, the fast-paced progress in the synthesis of novel materials possessing unprecedented and diverse functions has been key to the emergence of new technologies responding to the needs of society. Toward this end, compositional and structural complexity has been exploited to design materials exhibiting specific properties for target applications.^[1] The early attempts, starting from the Bronze Age, took root in a “base element” paradigm, that is, by diluting one or rarely two base elements with traces of doping elements to improve the performance of composites. However, the accessible base elements were just a few, including copper, iron, or nickel, severely limiting the design space.

Two decades ago, a different concept was proposed being focused on exploiting the previously unexplored structural configuration of multi-element with high concentrations, which is in stark contrast to conventional trace doping strategy. In particular,

this approach probes into the central region of the multi-element phase diagram, not in the edges or corners.^[2] In these classes of compounds, entropy plays a crucial role as it can be used as a key parameter to tune the overall material thermodynamic, kinetic, and structural features.^[3–5] In particular, the combination of multiple elements of single-phase crystal structures in equimolar or near-equimolar quantity are merged to form a new class of materials defined by the number of constituting elements (n),^[6] named medium/high-entropy materials (MHEMs), where medium and high refer to $3 \leq n < 5$ and $n \geq 5$, respectively (Figure 1a). Such a broad material family spans from metallic alloys to intermetallic and ceramic compounds, as well as microstructures with any number and any type of these phases.^[7–10] Importantly, the modulation of entropy by integrating species with different atomic radii, electronegativity, ionization energy, etc., enables defectiveness, distortions, structural stabilization, and cocktail effects that lead to finely tunable properties in MHEMs,^[11] making them a promising versatile platform for a broad range of applications, including energy storage and conversion, optoelectronics, catalysis.^[12] In contrast to bulk MHEMs, in which entropy engineering represents an established tool for attaining in-demand properties, its exploitation in the realm of 2D materials, mainly governed by single/two-element structures, is still at a nascent stage.

H. Mei, Y. Zhang, S. Yang
Frontiers Science Center for Transformative Molecules
School of Chemistry and Chemical Engineering
Shanghai Jiao Tong University
Shanghai 200240, China
E-mail: sheng.yang@sjtu.edu.cn

P. Zhang
State Key Laboratory of Material Processing and Die & Mould Technology
School of Materials Science and Engineering
Huazhong University of Science and Technology
Wuhan 430074, China

A. G. Ricciardulli, P. Samori
University of Strasbourg
CNRS
ISISUMR 7006
Strasbourg 67000, France
E-mail: ricciardulli@unistra.fr; samori@unistra.fr

 The ORCID identification number(s) for the author(s) of this article can be found under <https://doi.org/10.1002/advs.202409404>

© 2024 The Author(s). Advanced Science published by Wiley-VCH GmbH. This is an open access article under the terms of the [Creative Commons Attribution](#) License, which permits use, distribution and reproduction in any medium, provided the original work is properly cited.

DOI: 10.1002/advs.202409404

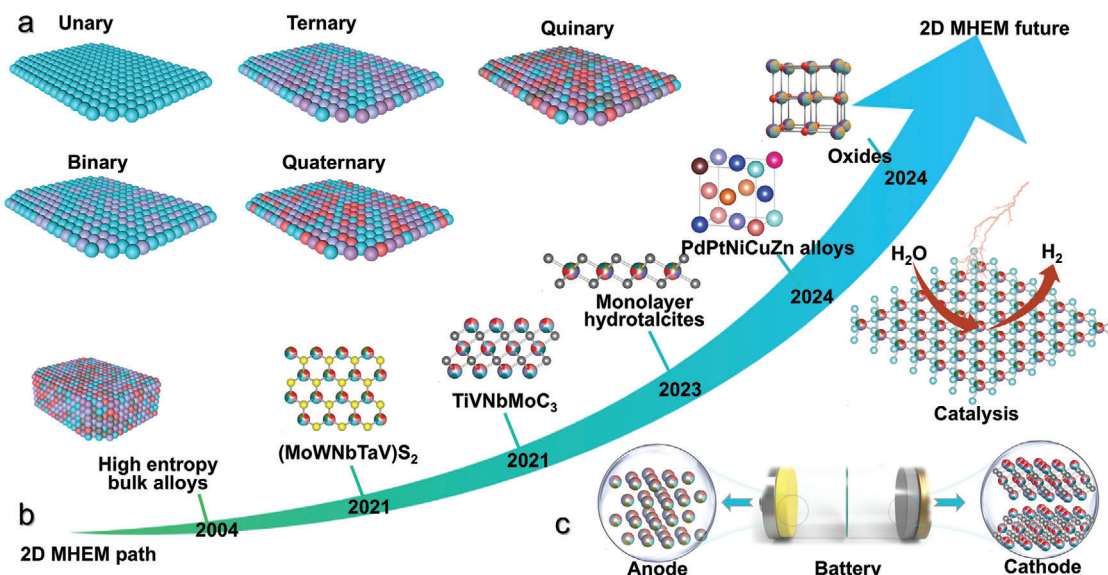


Figure 1. Schematic illustration of 2D MHEMs. a) Conceptual graphs from low entropy to high entropy. b) The development path of representative 2D MHEMs, such as MXene, sulfides, hydroxalclites and oxides. c) The energy storage and catalysis applications of 2D MHEMs.

2D materials are widely defined as sheet-like nanomaterials characterized by a lateral size exceeding 100 nm and a thickness below 10 nm.^[13] Due to their atomic scale thickness, 2D materials boast a range of unique advantages, such as large surface area, superior mechanical strength, and ease of property modulation via surface engineering.^[14] Recently, efforts have been dedicated to the design of functional 2D materials through entropy engineering (i.e., 2D MHEMs). A series of MHEMs architectures down to the 2D limit have been developed so far, being based on transition metal chalcogenides (TMC), alloys, metal-organic frameworks (MOF), MXenes, and hydroxalclites (Figure 1b,c).^[15–17] At such low dimensionality, due to quantum confinement, the medium/high-entropy effect is expected to heavily affect the lattice framework and thus the properties of complex 2D materials. For instance, versatile electromagnetic properties, such as superconductive behavior, metal-insulator transition, and antiferromagnetic transition, were detected in 2D high-entropy $(\text{CoAu})_{0.2}(\text{RhIrPtPd})_{0.8}\text{Te}_2$, $(\text{TiVCrNbTa})\text{S}_2$ and $(\text{MnFeCoNi})\text{PS}_3$.^[18] Thus, the integration of medium/high-entropy concepts and 2D structures holds the promise of creating a versatile library of materials with attractive physicochemical properties.

Previous review articles mainly discussed the theoretical property prediction of high-entropy 2D materials or potential applications of high-entropy van der Waals (vdW) materials.^[19,20] However, some key elements of 2D high-entropy materials, such as entropy engineering principles, crystal structural aberrations, and unique physicochemical properties, have not yet been reviewed in-depth. Herein, we comprehensively review the entropy engineering of 2D materials, including basic definitions, general materials categories, fundamental synthesis mechanisms, unique properties, and representative applications. Furthermore, the entropy stabilization effect, disordered multiple atomic distribution, and local electronic structure in 2D systems are thoroughly discussed. We also critically assess the advantages and

weaknesses of 2D MHEMs, providing an outlook on the key challenges and opportunities.

2. Theoretical Concept and Core Effects of 2D MHEMs

2.1. Thermodynamic Terminology

To avoid confusion and inconsistencies, choosing the right term for medium and high entropy for a wide set of materials is critical. In theory, the mixed entropy of a multi-component system consists of four fractions, as shown below:^[21]

$$\Delta S_{\text{mix}} = \Delta S_{\text{conf}} + \Delta S_{\text{vib}} + \Delta S_{\text{mag}} + \Delta S_{\text{elec}} \quad (1)$$

where ΔS_{conf} , ΔS_{vib} , ΔS_{mag} , and ΔS_{elec} are configurational entropy, vibrational entropy, magnetic dipole entropy, and electronic randomness entropy, respectively. Typically, configurational entropy attracts more dominant attention than its counterparts, which directly affects phase stability. However, to accurately determine the total entropy of a multi-component system, it is essential to account for contributions beyond ΔS_{conf} , such as ΔS_{vib} , ΔS_{mag} , and ΔS_{elec} . For instance, in the case of ΔS_{vib} , previous studies using finite-temperature ab initio methods have shown that while vibrational entropy can notably affect stability, its absolute magnitude does not always directly correlate with relative phase stabilities. Instead, the variation in vibrational entropy between different phases is more pertinent. Furthermore, it has been observed that vibrational entropy may decrease with increasing element diversity or number, complicating the prediction of its impact on phase stability. It should be noted that these considerations have been done mainly on alloys. Nevertheless, as the library of 2D MHEMs is broad and diverse, general calculations on vibrational entropy, magnetic dipole entropy, and

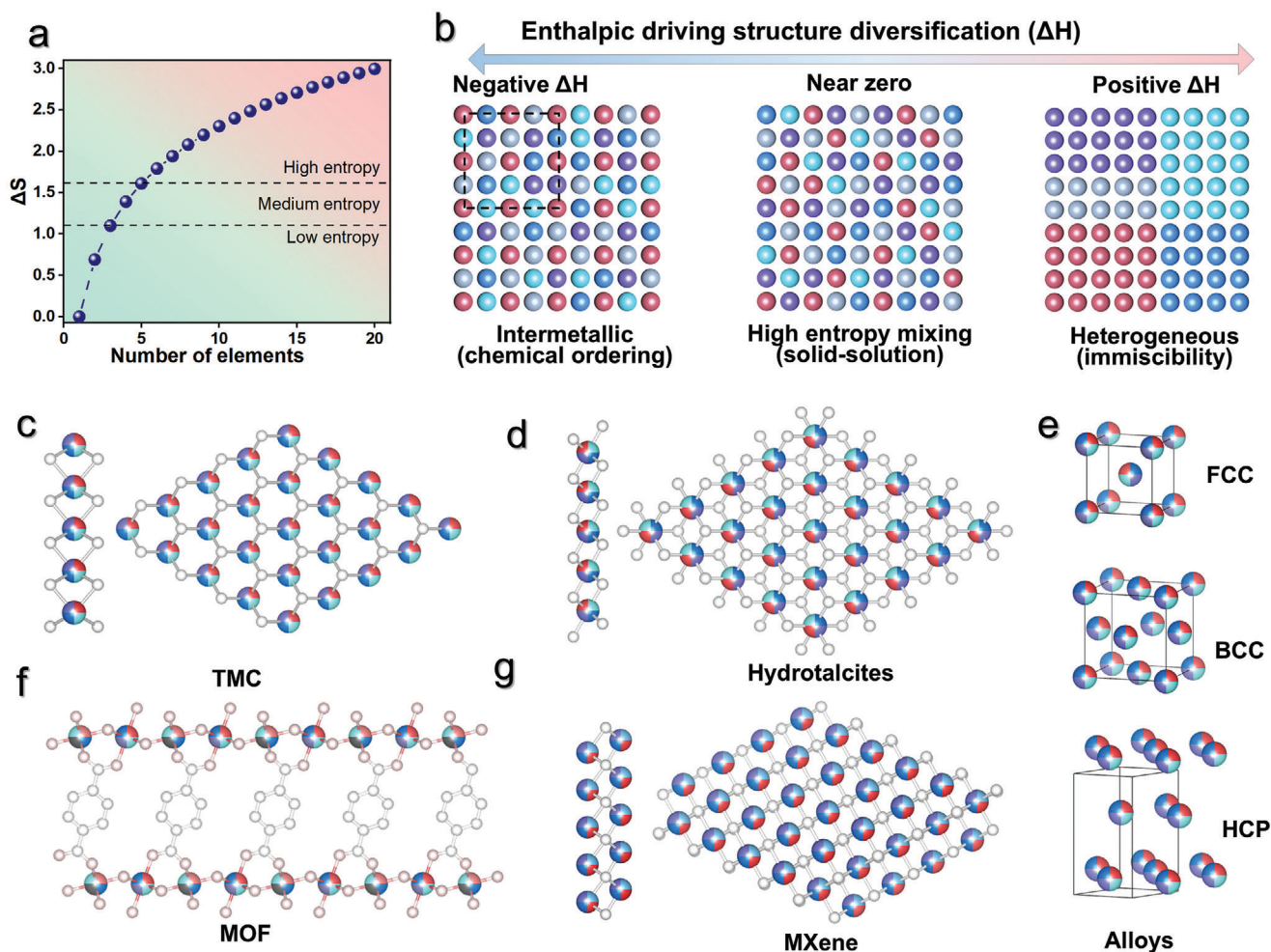


Figure 2. a) The configurational entropy under different numbers of elements, which is calculated based on Equation (3). b) Effect of enthalpy value on phase structure formation mechanism. c–g) Crystal structure of current reported 2D MHEMs, including TMC, MOF, MXene, hydrothermalites, and alloys with face-centered cubic (FCC), body-centered cubic (BCC), and hexagonal-close packed (HCP) structure.

electronic randomness entropy contribution are inherently challenging. Therefore, despite the role of the different entropy components, S_{conf} can be considered as the key factor. In a typical 2D MHEMs composed of metal and non-metal species, ΔS_{conf} can be written as the following equation:^[6]

$$\Delta S_{\text{conf}} = -R \left[\left(\sum_{i=1}^n X_i \ln X_i \right)_{\text{metal}} + \left(\sum_{j=1}^m X_j \ln X_j \right)_{\text{non-metal}} \right] \quad (2)$$

where R , X_i and X_j are the ideal gas constant, and molar content of metal and non-metal species, respectively. Obviously, the value of ΔS_{conf} increases with the element number. For traditional multi-components alloys with equimolar, $X = 1/n$, this Equation (2) can be simplified:

$$\Delta S_{\text{conf}} = R \ln n \quad (3)$$

with n as the number of elements. Based on theoretical calculations, at the equimolar ratio, the ΔS of unary, binary, ternary, quaternary, and quinary alloys are 0, 0.69, 1.10, 1.39, and 1.61R,

respectively. Thus, a number of researches have recommended a quantitative value of configurational entropy to distinguish medium (1.10–1.61R) and high entropy ($\geq 1.61R$), as shown in Figure 2a. Alternatively, MHEMs can be also defined by their compositions with disordered distribution, such as numbers of metal elements in equimolar or near-equimolar content (i.e., 3–4 and 5 or more metal elements represent medium entropy and high entropy, respectively).

In thermodynamic theory, the formation of 2D MHEMs is related to the interplay between entropy and enthalpy, expressed as the Gibbs free energy equation:

$$\Delta G_{\text{mix}} = \Delta H_{\text{mix}} - T \Delta S_{\text{mix}} \quad (4)$$

where T and ΔH_{mix} are temperature and enthalpy changes in mixing multiple elements. The interplay between ΔH_{mix} and $-T\Delta S_{\text{mix}}$, which are usually positive and negative, respectively, determines the resulting phase structure. On the one hand, the $-T\Delta S_{\text{mix}}$ depends on the number of elements and temperature, simultaneously serving as the driving force to achieve single

phase mixing, which is well-known as the “entropy stabilization effect”.^[22] On the other hand, enthalpy primarily hinges on properties of constituent elements, also directly influences the phase structure under near-equilibrium conditions.^[11] As shown in Figure 2b, the intermetallic compounds with highly ordered element distribution are favored with a negative value of ΔH_{mix} . In contrast, at positive ΔH_{mix} values, phase separation occurs, yielding heterogeneous structures. It is worth noting that for the near-zero value of ΔH_{mix} , a mixture of medium and high entropy is generally obtained. Furthermore, temperature is also a crucial physical parameter, which significantly influences the element distribution and crystal structure. In this regard, a detailed discussion will be provided in the section on synthetic methods.

2.2. Core Effects of 2D MHEMs

Entropy theory has been extensively employed for the design and synthesis of diverse functional 2D MHEMs (Figure 2c–g), including transition metal chalcogenides and halides, MOFs, MXenes, and hydroxalicates. To date, it has been discovered that the produced 2D MHEMs inherit core effects of traditional bulk forms, such as sluggish-diffusion effects, drastic-lattice distortion, and cocktail effects.^[23] Besides, as MHEMs thickness approaches the single-unit-cell limit, the possibility of discovering unusual quantum phenomena and exotic chemical properties is greatly enhanced due to quantum-confinement effects, strongly influencing the material properties. The drastic-lattice-distortion effects directly alter the structural properties and shape diverse defects like point, line, and interface defects.^[24] When coupled with atomic-thickness effects, these structural aberrations are further amplified, leading to strong surface lattice strain of 2D MHEMs. The sluggish-diffusion effects reduce internal atomic migration and similarly decelerate phase transformations.^[25] The cocktail effects denote a form of synergistic outcome arising from the interaction among diverse elements.^[26] A detailed description of these effects and their impacts on the properties of the material are provided in the following sections.

2.2.1. Drastic-Lattice-Distortion Effects

MHEMs require the integration of diverse elements into a single-phase lattice structure. Once elements with different atomic radius, chemical valences, and electronegativities coexist in a shared sublattice, the lattice distortion and strain emerge thereby altering the overall properties of MHEMs.^[27] Generally, the lattice distortion and strain increase as the disparity among elements widens. While the lattice strain of the localized lattice area may be minor, the cumulative effect on the long-range scope is substantial and consequential. For instance, research on alloys has shown that a 1% interatomic spacing change is likely to cause approximately a 12% variation in interatomic force.^[28] To date, the prevalent depiction of lattice distortion usually focuses on the atomic radius differences (δ), which can be directly evaluated by the following formula:^[29]

$$\delta = 100 \sqrt{\sum_{i=1}^n C_i \left(1 - \frac{r_i}{\bar{r}}\right)^2}, \quad \bar{r} = \sum_{i=1}^n c_i r_i \quad (5)$$

where n , r , and c_i are the number of elements, atomic radius, and concentration of constituent element i , respectively. Several studies have shown that this parameter is valid for estimating phase stability of high-entropy materials.^[30] When scaling down the crystals from bulk to the 2D space, the lattice distortion may be further strengthened. Therefore, a number of structural defects, such as vacancies, grain boundaries, and dislocations have been discovered in 2D MHEMs.^[23]

2.2.2. Atomic-Thickness Effects

The atomic-thickness effects impart many unique characteristics to MHEMs that are different from typical bulk forms. First, the phonon/charge carriers of 2D MHEMs are confined to the atomic-thickness region, which is favorable for the development of ultrathin yet sensitive optoelectronic devices.^[31] Second, considering the strong lattice distortion limited at 2D scale, atomic strain and surface defects are highly possible. Third, the strong in-plane covalent bond and weak interlayer forces lead to substantial flexibility and mechanical strength, which make MHEMs promising flexible wearable electronics devices.^[32] Last but not least, atomic thickness endows materials with a large accessible surface area, which further enables high tunability of properties and functionalities via ingenious design by means of defect/phase/strain engineering.^[33] These remarkable characteristics offer advantages for applications propelled by surface chemical reactions like electrocatalysis, batteries, and sensing.

2.2.3. Cocktail Effects

The concept of cocktail effects, initially introduced by Ranganathan to depict amorphous alloys, gum metals, and high-entropy alloys, suggests that blending various elemental species may result in unexpectedly remarkable properties.^[34] In 2D MHEMs, the cocktail effect refers to the interaction of multiple constituent elements in MHEMs, resulting in superior performance.^[35] It emphasizes that the synergistic working effect dominates the properties of MHEMs rather than solely contribution from any of the specific elements. The interplay between diverse components can be significantly altered by the element types and stoichiometry, which further affect the material's properties. Additionally, it is highly feasible to achieve outstanding performance in MHEMs by replacing scarce and/or toxic elements with abundant and sustainable ones, thus contributing to sustainability.

2.2.4. Sluggish-Diffusion Effects

The sluggish-diffusion effect of 2D MHEMs refers to the migration of atoms in severely disordered lattices is limited. In general, MHEMs exhibit varying local energy in the sublattice area, attributed to various bonding types of constitute elements. Compared to the almost same diffusion barrier in conventional materials, the energy barrier along the atom diffusion pathway for MHEMs is continuous. Thus, during the internal migration of atoms, a high probability of falling into high-barrier sites occurs, named the “trapping effect”, significantly slowing down

Table 1. Representative examples of the reported 2D MHEMs.

MHEMs	Number of metallic elements	Metal contents [at. %]	Entropy Level	Ref
Alloys	3	43%Pd, 28%Pt, 29%Ag	medium	[37]
Alloys	5	23%Pt, 20%Pd, 17%Ir, 16%Ru, 24%Ag	high	[38]
Alloys	5	22%Fe, 22%Ni, 22%Co, 22%Cr, 11%Nb	high	[39]
MXene	5	7.1%Ti, 8.6%Nb, 6.6%Ta, 0.1%Cr, 4.9%V	high	[40]
MXene	3	33.3%Ti, 15% V, 1.7%Cr	medium	[41]
Hydrotalcites	5	3.31%Mn, 7.88%Fe, 4.16%Co, 8.54%Ni, 7.38%Cu	high	[42]
TMC	5	12%Co, 2% V, 2%Ni, 2%Mn, 2%Zn	high	[43]
TMC	5	12% Ru, 6%Ir, 8%Fe, 2%Co, 2%Ni	high	[44]

the diffusion rate.^[12] Furthermore, the sluggish atomic diffusion also influences the phase transformation rate. Recent studies have demonstrated that sluggish-diffusion effects stabilize the microstructure of MHEMs and alter their performance in applications. For instance, the dynamic stability of a 2D high-entropy electrocatalyst would be strengthened through sluggish-diffusion effects, enabling excellent catalytic performance even in harsh environments for extended periods.^[36]

3. Synthesis of 2D MHEMs

3.1. General Principles for Making 2D MHEMs

The controlled preparation of high-quality 2D MHEMs with desired composition, phase purity, and structure is key for practical applications. However, increasing the entropy of materials while retaining their 2D morphology represents the main challenge in the synthesis of this emerging class of low-dimensional materials. In terms of structural assembly, the typical synthesis mainly relies on bottom-up and top-down approaches. Bottom-up strategies rely on the controlled assembly of small molecules forming macroscale 2D frameworks. In contrast, top-down methods are generally based on the exfoliation of bulk materials using chemical, physical, and mechanical techniques. For the sake of entropy engineering of 2D materials, overcoming the intrinsic immiscibility of metal atoms driven by atomic radius difference, electronegativity disparity, and valence electron concentration is the most critical point. Representative examples of 2D MHEMs produced based on increasing the entropy of the host phase, including alloys, MXene, hydrotalcites, and metal sulfides are summarized in Table 1.^[37–44] The inherent properties of elements, including electronegativity, atomic/ionic radius, and electronic structure, should be carefully considered in designing the synthesis methods.

3.2. Methods to Increase the Entropy of 2D Materials

The designing methods to increase the entropy of 2D materials are usually based on doping and alloying strategies. The doping strategy involves directly mixing various metal precursors to acquire a medium/high-entropy structure (Figure 3a). Generally, oriented by a 2D lattice framework, all metal precursors totally dissolve and dope into to targeted lattice structure under extreme conditions. Alternatively, alloying by infiltrating other components into the target 2D monocomponent template represents another effective way to produce 2D MHEMs, as shown in Figure 3b. According to Gibb's free energy formula (Equation (4)), in addition to ΔS_{mix} and ΔH_{mix} , doping/alloying temperature constitutes a pivotal parameter, regulating the feasibility of medium/high-entropy systems. Ultrahigh doping/alloying temperatures and ultrafast heating rates were generally employed to achieve a stable homogeneously mixed solid-solution state, as the blending of metals with divergent characteristics is facilitated. For instance, the classical carbothermal shock synthesis was even conducted at 2000 K ultrahigh temperature and 10^5 K/s ultrafast heating rate.^[45] However, such extreme conditions do not allow structural control over the production of MHEMs in a 2D fashion. Thus, the currently reported synthetic methods to increase the entropy of 2D materials, such as wet-chemical synthesis, chemical vapor deposition (CVD) doping, and calcination alloying, are usually carried out under relatively mild conditions. In the following section, state-of-the-art synthesis methods will be introduced, with a focus on the impact of experimental parameters on the features including surface vacancies, lateral size, thickness, and phase structure of the materials.

3.2.1. Wet-Chemical Synthesis

Wet-chemical synthesis, including co-precipitation, solvothermal, and molten-salt reactions (Figure 4a,b), is the most

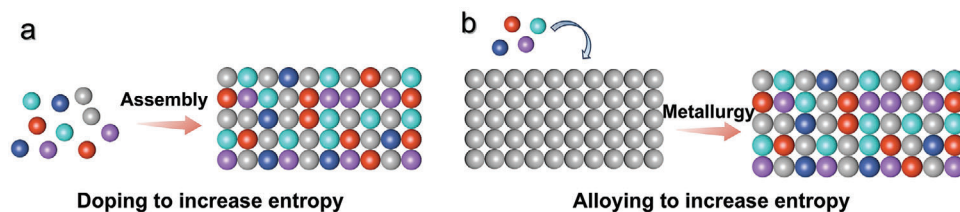


Figure 3. a) Doping strategy to increase the entropy of 2D materials. b) Alloying reaction for achieving medium/high entropy.

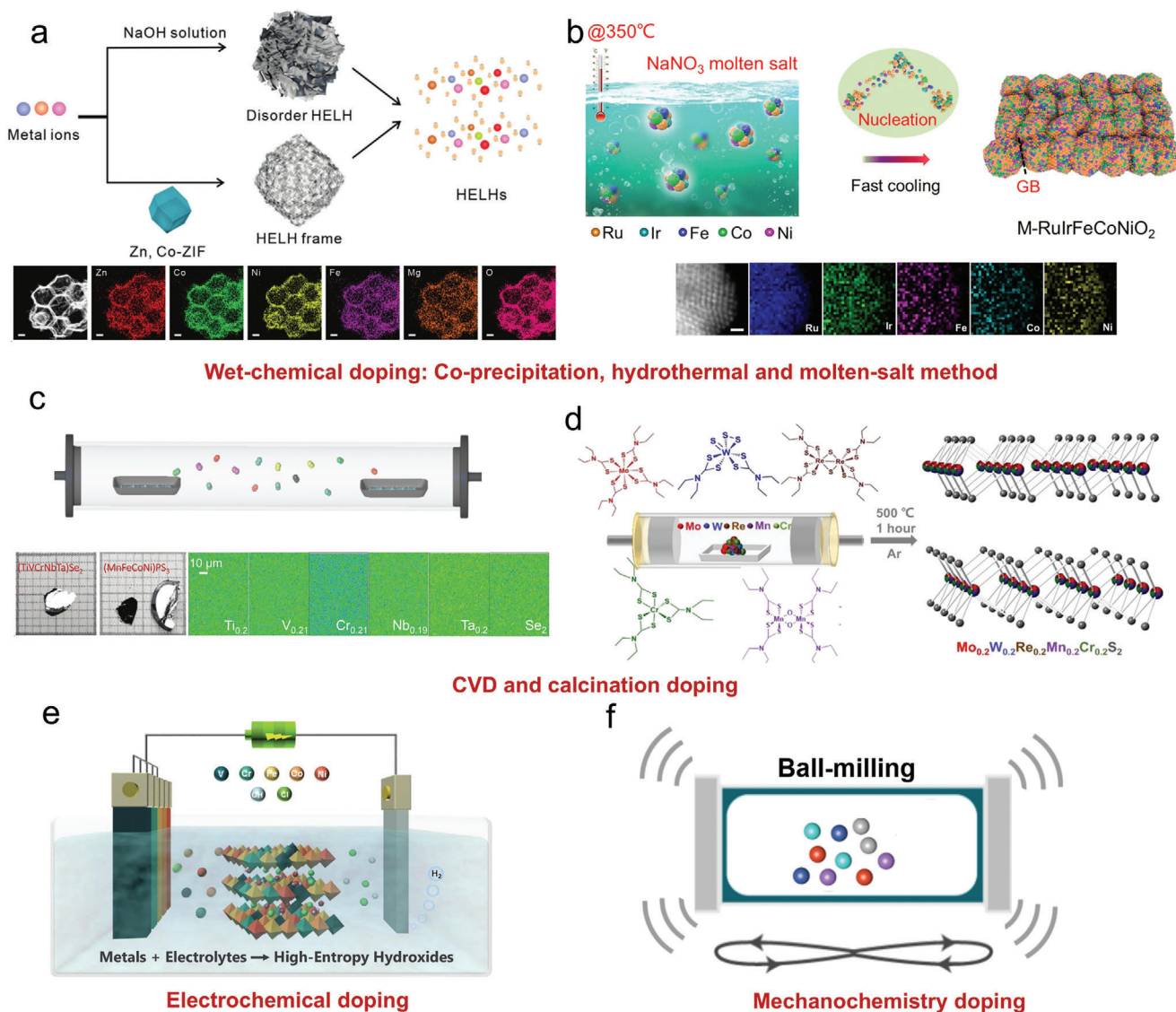


Figure 4. Doping synthesis to increase the entropy of 2D materials, including wet-chemical doping, chemical vapor deposition doping, electrochemical doping, and mechanochemistry doping. a) Wet-chemical etching of Zn/Co-MOF to prepare high-entropy hydroxides. Reproduced with permission.^[52] Copyright 2023, Wiley-VCH. b) Molten-salt synthesis of 2D high-entropy RuIrFeCoNiO₂. Reproduced under the terms of the CC-BY-NC licence.^[44] Copyright 2023, AAAS. c) CVD synthesis of MHEMs monocrystal, including Metal dichalcogenides, halides, and phosphorus trisulfides. Reproduced with permission.^[18] Copyright 2021, American Chemical Society. d) Calcination synthesis of 2D high-entropy Mo_{0.2}W_{0.2}Re_{0.2}Mn_{0.2}Cr_{0.2}S₂. Reproduced with permission.^[55] Copyright 2023, Wiley-VCH. e) Direct electrodeposition synthesis of high-entropy hydroxides. Reproduced with permission.^[57] Copyright 2022, Elsevier. f) Mechanochemistry doping synthesis.

frequently-used strategy to produce 2D MHEMs.^[46,47] In order to promote co-precipitation and solvothermal process, a stoichiometric ratio of various metal salts is dissolved in a specific solvent to form a mixture. Then the homogeneous solution is transferred into an autoclave to complete the synthesis. Generally, the synthesis of 2D MHEMs is based on a typical crystallization mechanism, which involves crystal nucleation and subsequent growth.^[46] The crystal nucleation is generated by the spontaneous random aggregation of ions at a supersaturating state. On the basis of thermodynamics theory, this process needs to cross the free energy barrier affected by the reaction temperature. Based on LaMer theory, the fast nucleation is conducive to reach

a single-phase solid solution structure and higher entropy.^[48] On the contrary, the slower nucleation may lead to phase separation and decreased configurational entropy. The subsequent growth has important effects on the resulting crystallinity, morphology, and size, which can be regulated by surfactants. A variety of 2D medium/high-entropy hydroxides are synthesized by co-precipitation or solvothermal doping. The hydroxide crystal structure presents sufficient flexibility to endure the mismatching of metal ion radius and coordination states. Considering the 133 pm radius of hydroxyl ion, the metal ion radius is in the range of 55 to 88 pm, to ensure the octahedral structure stability of metal hydroxides.^[49] Currently, a maximum of nine metal

elements can co-exist in the hydroxide structure framework, and the obtained novenary hydroxide still presents ultrathin thickness. Analogously, the multiple metal ions can also co-exist in MOF.^[50] Previous works have demonstrated the conformal conversion of MOF into hydroxides, oxides, and sulfides.^[51] With this respect, Tang et al. reported the preparation of high-entropy hydrotalcites via etching Zn/Co-ZIF in a polymetallic mixing solution (Figure 4a).^[52] The prepared high-entropy hydrotalcite presented 1.07 nm thickness, hollow frame structure, and amorphous features.

Compared to co-precipitation or solvothermal methods, molten salt-assisted synthesis is carried out at a higher temperature and heating rate. Thus, the guest metal ions are more easily doped into the host phase structure to achieve medium/high-entropy mixing. For instance, Huang et al. reported the introduction of Ni/Co/Fe/Ir ions into RuO₂ crystal structure under NaNO₃ molten salt and successfully produced 2D high-entropy (FeCoNiIrRu)O₂ with 3 nm thickness.^[44] The synthesis was carried out under rapid high-temperature mixing and fast cooling, the high-entropy (FeCoNiIrRu)O₂ still presents many defects induced by lattice-distortion effects, such as vacancies and grain boundaries. In addition to hydroxides and oxides, a large class of Pd-based alloys with face-centered cubic structures can be synthesized through the reduction of metal salts in wet-chemical conditions.^[53] However, these Pd-based alloys produced by direct co-reduction synthesis all present quasi-2D features, whose lateral size is in the range of 50–200 nm. In general, the wet-chemical doping synthesis is currently applicable to limited materials such as hydrotalcites, oxides, and Pd-based alloys.

3.2.2. CVD and Calcination Doping

Calcination and CVD doping are alternative effective synthetic techniques (Figure 4c,d), which are mainly performed for making high-entropy MAX phases and TMC. CVD is a conventional synthetic technique that uses a carrier gas at high temperatures to yield highly crystalline materials at the interface with a substrate. In contrast, calcination is a process that occurs through solid or liquid reactions to assemble species with high-entropy mixing. Many experimental parameters, such as substrate interface, heating rate, reaction time, cooling rate, and gas atmosphere, have great impacts on the calcination process and final products. Considering the higher reaction temperature and ramping rate, various metal ions are more likely to integrate with ordered crystal domains rather than in a random fashion through wet-chemical doping. The typical calcination process was often employed for the preparation of MAX phases by solid phase reactions. Huang et al. reported the synthesis of medium/high-entropy M₂SnC (M = Ti/V/Nb/Zr/Hf) MAX phases using metal powder and carbon as starting reagents.^[54] In order to overcome the incompatibility between the multiple components, the whole process was conducted at 1350 °C under 30 MPa. Besides, using metal dithiocarbamate as a precursor, Lewis et al. performed the rapid synthesis of high-entropy Mo_{0.2}W_{0.2}Re_{0.2}Mn_{0.2}Cr_{0.2}S₂ nanosheets via calcination process (Figure 4d).^[55] Different from calcination, CVD represents another effective method to yield high-quality single-crystal 2D materials. For example, Hosono et al. synthesized a series of high-entropy layered materials via CVD doping,

including mixed metal dichalcogenides, halides, and phosphorus trisulfides, which greatly expanded the library of 2D MHEMs (Figure 4c).^[18] The chemical/physical exfoliation process was essential to exfoliate MAX crystal or bulk TMC into 2D sheets. In general, the chemical etching of MAX performed in HF or F-containing etching solution led to mixed surface terminations including –F, –O, and –OH.^[56] Unlike the chemical etching process of MAX, the weak interlayer interaction of TMC can be eliminated by mechanical force, such as the scotch tape and ball-milling methods.

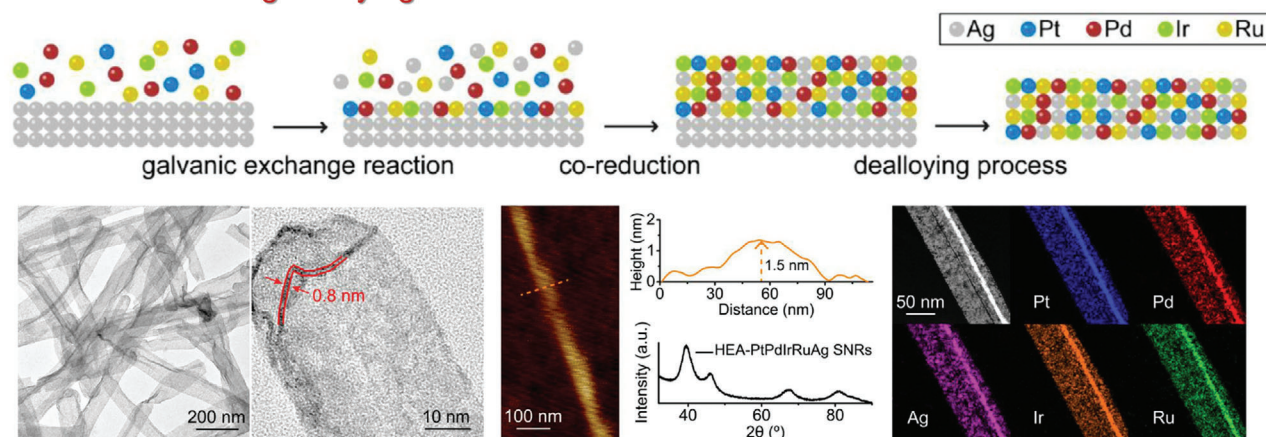
3.2.3. Electrodeposition Doping

Electrodeposition is a cost-effective and scalable synthetic method. As shown in Figure 4e, the electrodeposition system includes an electrochemical workstation, an electrolytic tank, the electrolyte, and electrodes. The reactants in the electrolyte are oxidized or reduced upon the application of a potential, and continuously deposited on the working electrode. Therefore, the crystal nucleation and subsequent growth of target materials can be controlled by changing the electrodeposition mode (DC/pulse), overpotential, solution viscosity, and stirring speed, thus obtaining different film morphologies and deposition sizes. The redox potential of various metal ions is a key to increasing the entropy of materials via electrodeposition doping. In general, the high potential will promote fast deposition of metal ions onto the electrode surface, achieving a high-entropy mixing. In this regard, Dong and coworkers developed a universal and low-cost solution electrodeposition approach for producing high-entropy layered CoFeVCrNi-LDH (Figure 4e).^[57] The whole process was conducted in a two-electrode system using metal foil (Co/Fe/V/Cr/Ni) and Pt plate, as anode and cathode, respectively. A series of 2D MHEMs were produced, including ternary CoFeNi-LDH, pentabasic CoFeNiMnCr-LDH, senary CoFeNiZnCrAl-LDH, octonary CoFeNiZnCrAlCuMn-LDH, demonstrating the general applicability of such electrochemical synthesis. Alternatively, the work from Reza et al. provided further evidence of high-yield synthesis of high-entropy (FeMnNiCaMg)_xOH_y at a high current density of 232 mA/cm².^[58]

3.2.4. Mechanochemistry Doping

Mechanochemistry doping refers to the use of mechanical energy to trigger chemical reactions, such as the ball-milling technique (Figure 4f). Generally, guest metal species are introduced into a host crystal structure under high mechanical force, resulting in a high-entropy state. Recently, due to the recent progress in the modernization of mechanical equipment, mechanochemical synthesis with solvent-free and eco-friendly attributes is rapidly emerging as a promising alternative for the scalable production of MHEMs. Nevertheless, to overcome the immiscibility of diverse elements and trigger their mixing, mechanochemical synthesis should be coupled with other methods, such as heat and optical radiation. Dai et al. performed a class of mild mechanochemical coupled with calcination reactions for preparing high-entropy K_{1-x}Na_x(MgMnFeCoNi)F₃ perovskite fluorides

a Atomic exchange alloying



b Liquid metal assistant to increase entropy

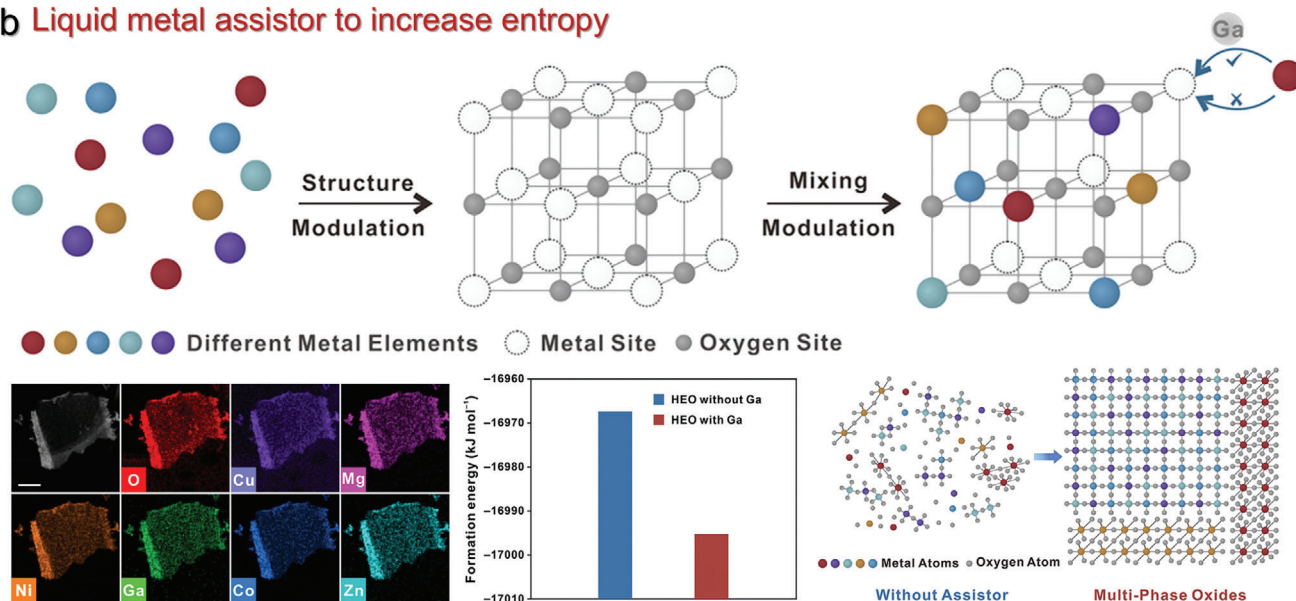


Figure 5. a) Atomic exchange alloying reactions to increase entropy. The high-entropy AgPtPdIrRu nanoribbon was synthesized based on the Ag template. Reproduced with permission.^[38] Copyright 2022, American Chemical Society. b) Preparation of 2D high-entropy oxides by doping multifarious metal precursors with liquid Ga assistant. Clearly, the Ga assistant reduced the formation energy of high-entropy oxides and inhibited phase separation. Reproduced with permission.^[63] Copyright 2024, American Chemical Society.

and $(\text{CeZrHfTiLa})\text{O}_x$ fluorite oxides.^[59] Likewise, Li et al. synthesized medium-entropy NiZrCu- H_2BDC -MOF with an average thickness of 4 nm via ultrasonic-assisted approaches.^[60]

3.2.5. Atomic Exchange Alloying

Alloying or metallurgy is a classic approach to increasing the entropy of 2D materials. In this process, the initial metal template reacts with other metal sources due to the difference in reduction potential. For instance, Guo et al. introduced a universal synthesis technique to prepare high-entropy alloys on an Ag nanowires-based template (Figure 5a).^[38] The formation process of high-entropy alloy is composed of three steps: 1) initial nucleation via galvanic ion exchange process induced by the reduc-

tion potential difference; 2) subsequent crystal growth by continuous co-reduction of metal sources; 3) dealloying process by nitric acid. In contrast to high-temperature metallurgy, the galvanic ion exchange process was carried out in the liquid phase at 200 °C. Furthermore, senary PtPdIrRuAuAg, septenary PtPdIrRuAuRhAg, and octonary PtPdIrRuAuRhOsAg nanoribbons with 1.5 nm thickness, 50–150 nm width, and micronmeter-scale length, were successfully synthesized. Analogously, Skrabalak et al. reported the alloying process for the preparation of single-phase high-entropy alloys (Pd, Sn, Ag, Co Cu, Pt, Ni, and Au components). Initially, bimetal PdCu and AuCu alloys were employed as fundamental cores and coated by other shell metals (Pt, Ni, Co et al.) via a co-reduction process.^[61] After subsequent annealing, the core-shell metal precursor was transformed into high-entropy alloys due to internal galvanic exchange reactions.

Noteworthy, the relative redox potentials (E_{red}) of metal determine internal galvanic exchange reactions. Thus, the metal with high E_{red} tended to replace the one with lower E_{red} .

3.2.6. Other Synthetic Methods

Many other synthetic approaches including magnetron sputtering and liquid metal assisted synthesis have recently emerged to prepare 2D MHEMs. Yang et al. introduced advanced magnetron sputtering to yield 2D metals on modified polyvinyl alcohol substrates and demonstrated the general synthesis of Ti, medium-entropy ZrCuAlNi alloys, high-entropy FeCoNiCrNb alloys.^[39] Noteworthy, the obtained 2D medium/high-entropy alloys were endowed with amorphous characteristics, micrometer-scale lateral size, and thicknesses down to a few tens of nanometers. The thickness, crystallinity, and components of 2D alloy film can be effectively controlled by regulating several magnetron sputtering parameters, such as sputtering power and gas flow rate. Besides magnetron sputtering, Fu et al. found liquid Ga could assist in overcoming the elemental immiscibility, enabling the production of a broad variety of high-entropy alloys in the form of nanoparticles under relatively mild conditions.^[62] In recent work, they showed the possibility of extending such a synthetic strategy to yield a series of 2D high-entropy oxides with phase controllability, including rock-salt, spinel, perovskite, and fluorite structures, as shown in Figure 5b.^[63] According to density functional theory calculations (DFT), liquid Ga reduced the formation energy of high-entropy oxides, inhibiting phase separation. From a broader perspective, liquid metal might be used to extend the family of high-quality 2D MHEM, such as carbides and sulfides.

3.2.7. Comparison of Various Synthesis

The controllable preparation of high-quality 2D MHEMs with desired composition, phase structure, and morphology is of great importance for the further development of the field. Wet-chemical methods are widely used for synthesizing a variety of 2D MHEMs, including hydrotalcites, oxides, and sulfides. By designing experimental parameters such as reaction temperature, time, and solvent systems, the nanosheet size and phase structure can be effectively controlled. In general, wet-chemical synthesis is performed in mild conditions and does not require sophisticated equipment. Nonetheless, current approaches are affected by low yield and lack of controlled atomic distribution. In contrast, CVD and calcination strategies can be used to form high-quality 2D MHEMs with excellent phase purity and tunable morphology. However, this method requires advanced equipment and high energy consumption. As a result, upscaling is severely hindered. Besides, mechanochemical methods, electrodeposition and magnetron sputtering have been reported for synthesizing 2D MHEMs. Nevertheless, these methods are still in their infancy. A major challenge in mechanochemical synthesis is obtaining high-quality 2D sheets with controlled thickness and size. So far, electrodeposition and magnetron sputtering are still limited to the synthesis of a limited class of materials, such as hydrotalcite or alloys. In perspective, further efforts are needed to enhance the intermixing of components while keeping a 2D architecture.

4. 2D MHEMs Structure and Properties

Up to now, numerous 2D MHEMs have been produced via multifarious advanced synthetic technologies. Despite distinct differences in components, chemical bonding, and phase structures, the family of 2D MHEMs can be classified into layered and non-layered architectures. The typical examples of 2D layered MHEMs are MXene and hydrotalcite, which possess strong in-plane covalent bonds and weak interlayer Van der Waals (vdW) forces. On the contrary, although a number of MHEMs are endowed with non-layered structures, their atomically thin analogues can be synthesized by bottom-up approaches, such as Pd-based metallene and metal oxides. In this section, we will discuss the structural aberrations and the related physicochemical properties of 2D MHEMs.

4.1. Severe Crystal Structure Distortion

The properties of 2D MHEMs largely depend on their phase structure and elemental composition. In contrast to traditional low-entropy 2D materials with fixed bond length, 2D MHEMs usually exhibit tunable bond length and strength, induced by disordered atomic distributions and atomic sizes, which further affect the 2D microstructure. As shown in Figure 6a–c, drastic-lattice-distortion effects of 2D MHEMs lead to the formation of tensile and compressive strain. In localized lattice, tensile strain induces lattice expansion, while compressive strain triggers lattice contraction. When the lattice strain is too strong for the 2D structure to withstand, the crystal structure will change dramatically, leading to the formation of grain boundary, phase separation, or polycrystalline structure (Figure 6d). For instance, Song et al. reported Rietveld refinement of XRD data to investigate the crystal structural aberration in high-entropy $\text{Co}_x(\text{VMnNiZn})_{1-x}\text{PS}_3$.^[43] As shown in Figure 6e, the internal P-P bond length of $\text{Co}_x(\text{VMnNiZn})_{1-x}\text{PS}_3$ changed with Co content. Obviously, the original CoPS_3 delivers a lower P-P bond length than that of high-entropy $\text{Co}_x(\text{VMnNiZn})_{1-x}\text{PS}_3$. Furthermore, the discrepancy of (001) full width at half-maximum (FWHM) between CoPS_3 and high-entropy $\text{Co}_x(\text{VMnNiZn})_{1-x}\text{PS}_3$ also demonstrated lattice distortion (Figure 6f). At different Co contents, the lattice constant a of $\text{Co}_x(\text{VMnNiZn})_{1-x}\text{PS}_3$ was significantly different (Figure 6g). By comparison, high-entropy $\text{Co}_x(\text{VMnNiZn})_{1-x}\text{PS}_3$ presented a larger lattice constant, indicating tensile structure along an axis. Meanwhile, the lattice strains of $\text{Co}_x(\text{VMnNiZn})_{1-x}\text{PS}_3$ were all calculated based on Williamson–Hall (W–H) analysis. As shown in Figure 6h, the lattice strain ϵ enhances gradually with the decrease of Co content. The in-depth analysis of $\text{Co}_x(\text{VMnNiZn})_{1-x}\text{PS}_3$ lattice proved the structural aberrations induced by high-entropy effects.

4.2. Abundant Defects and Atomically Lattice Strain

Similar to high-entropy $\text{Co}_x(\text{VMnNiZn})_{1-x}\text{PS}_3$, structural aberrations were also inspected in other 2D MHEMs, such as high-entropy $(\text{Ti}_{1/5}\text{V}_{1/5}\text{Zr}_{1/5}\text{Nb}_{1/5}\text{Ta}_{1/5})_2\text{AlC}$ MAX phase and the derived MXene.^[64] As shown in Figure 7a, numerous transparent

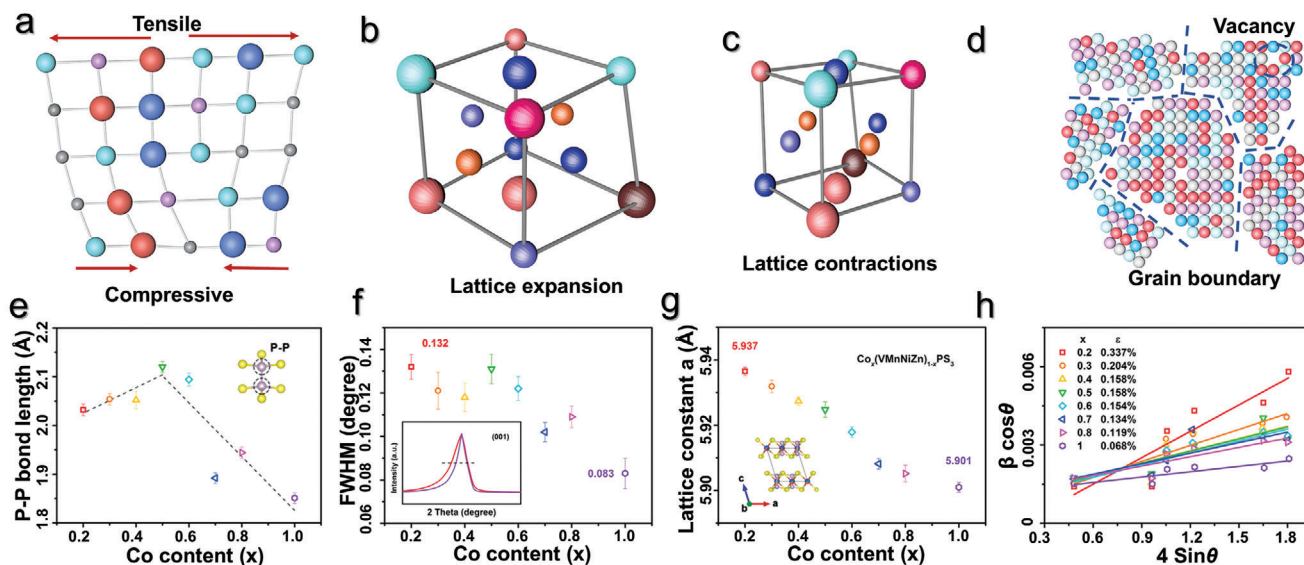


Figure 6. Structural aberrations of 2D MHEMs. a) Atom discrepancy induces structure compressive and tensile strain. b) Lattice expansion induced by tensile strain; c) Lattice contractions induced by compressive strain; d) Grain boundary and vacancy caused by severe lattice distortion. The crystal structure of 2D high-entropy $\text{Co}_x(\text{VMnNiZn})_{1-x}\text{PS}_3$ is regarded as an illustrative example. e) P–P bond length at different Co content. f) (001) plane full width at half-maximum varies with Co content. g) The lattice constant a varies with Co content. h) Lattice strain ϵ calculated based on W–H analysis. Adapted with permission.^[43] Copyright 2022, American Chemical Society.

and twisted nanosheets were observed in TEM images. In addition, the microstructure of 2D high-entropy MXene, including strong lattice mismatch and defects, was also revealed (Figure 7b). Furthermore, using atomic-resolution high-angle annular dark-field images, geometric phase analysis was performed to demonstrate the distribution of lattice strain. As displayed in Figure 7c, compressive and tensile strain were both

identified. Despite the strong lattice strain, the crystal structure and ultrathin nanosheet morphology was preserved. In addition to the discovery of lattice strain, the grain boundary was also detected in 2D MHEMs. For example, Huang et al. prepared misoriented high-entropy RuIrFeCoNiO_2 , which exhibited uniform 2D morphology with 3 nm thickness and abundant grain boundaries (Figure 7d–f).^[44]

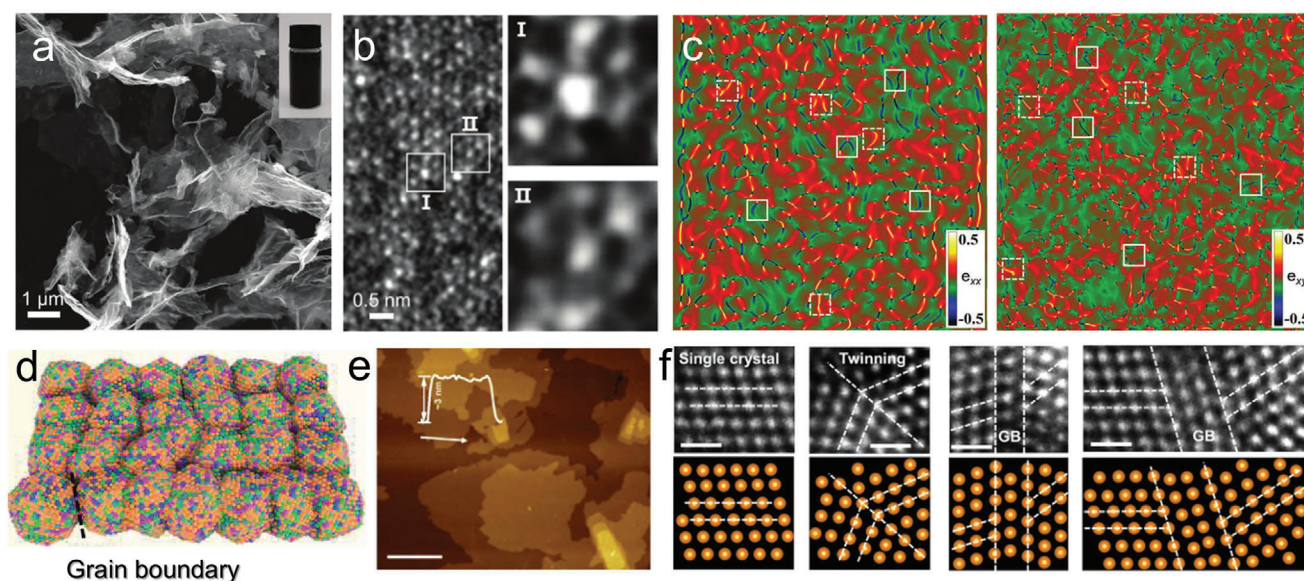


Figure 7. Structural features of 2D MHEMs. a,b) SEM and TEM images of high-entropy $(\text{Ti}_{1/5}\text{V}_{1/5}\text{Zr}_{1/5}\text{Nb}_{1/5}\text{Ta}_{1/5})_2\text{AlC}$ derived MXene. Defects induced by lattice distortion are clearly observed. c) Strain distribution of high-entropy MXene along e_{xx} and e_{xy} direction. A number of atomic lattice strains were detected. Reproduced with permission.^[64] Copyright 2021, Wiley-VCH. d–f) Structure, AFM, and STEM images of 2D high-entropy RuIrFeCoNiO_2 (scale bar: 2 μm for e, 0.5 nm for h). The RuIrFeCoNiO_2 delivers 3 nm thickness and abundant grain boundaries. Adapted under the terms of the CC-BY-NC licence.^[44] Copyright 2023, AAAS.

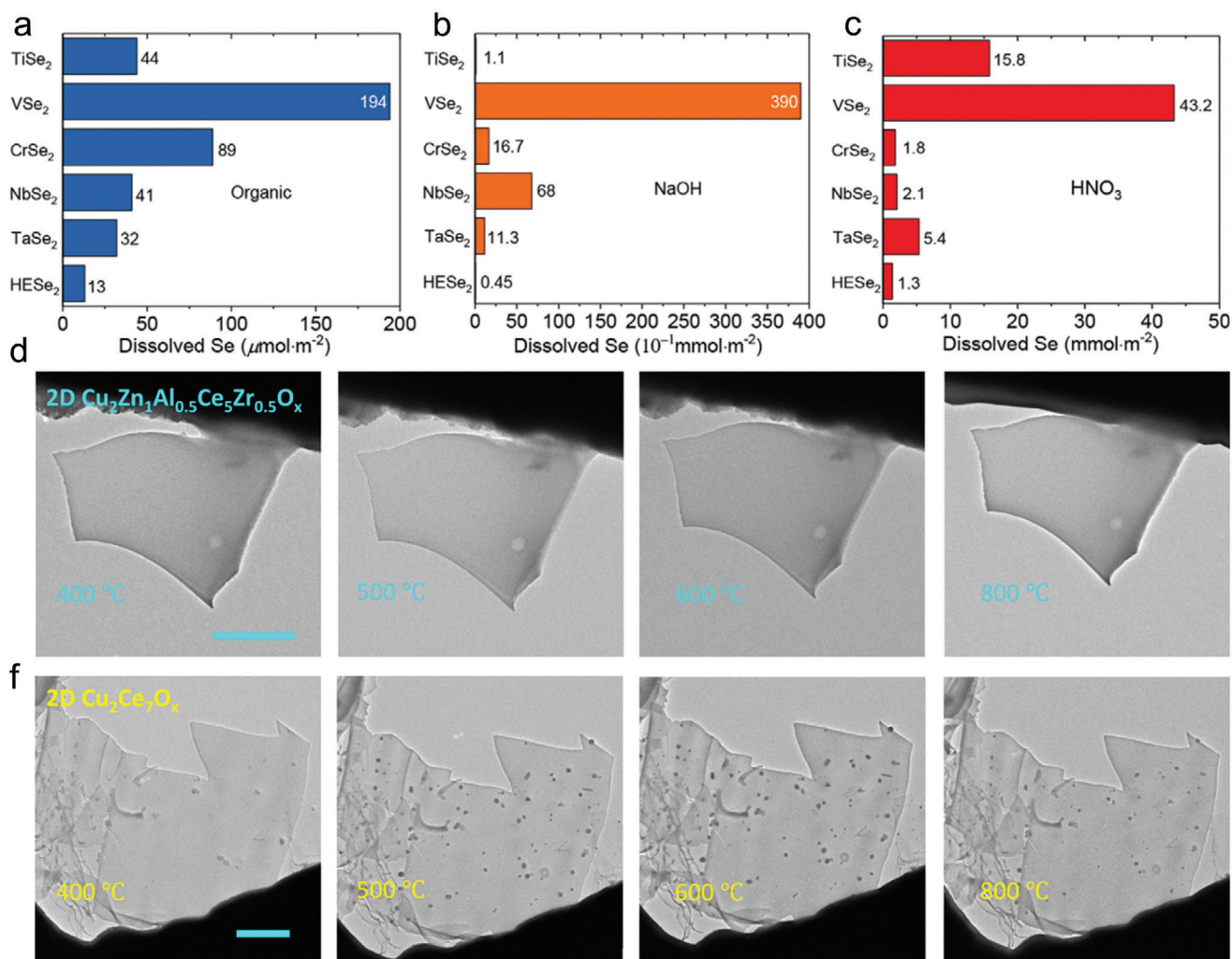


Figure 8. The strong structural stability of 2D MHEMs. a–c) Corrosion resistance comparison between high-entropy (Ti, V, Cr, Nb, Ta)Se₂ and parallel monocomponent under HNO₃, NaOH, and organics conditions. Reproduced with permission.^[18] Copyright 2021, American Chemical Society. d–f) In situ TEM images of 2D high-entropy Cu₂Zn₁Al_{0.5}Ce₅Zr_{0.5}O_x and Cu₂Ce₇O_x for reverse water gas shift reaction in range of 400–800 °C. Reproduced under the terms of the CC-BY-NC licence.^[66] Copyright 2023, Springer Nature.

4.3. Enhanced Structural Stability

The entropy engineering could significantly affect the structural stability of 2D materials. The strong lattice distortion would create high energy barriers, slowing down atom diffusion, and resulting in superior thermal stability, mechanical strength, and corrosion stability. As shown in **Figure 8a–c**, corrosion resistance of 2D high-entropy (Ti, V, Cr, Nb, Ta)Se₂ tests were conducted in HNO₃ (8.1 m, 10 min), NaOH (0.5 m, 10 min) and n-butylamine (1.0 mmol butylamine and 2 mL tetrahydrofuran mixing solution, 1 h).^[18] 2D (Ti, V, Cr, Nb, Ta)Se₂ exhibited lower concentrations of dissolved Se than its counterparts, indicating enhanced corrosion resistance and higher stability. In practical applications, the irreversible leaching and corrosion of metal active sites remain still challenging. Shao et al. reported the high-entropy effect confers 2D FeCoMoWO_x self-healing behavior in oxygen evolution reaction (OER).^[65] In a borate buffer containing cobalt ions condition, 2D FeCoMoWO_x shows an overpotential

reduction behavior and long-term stability of 100 h in catalysis. In addition to the corrosion resistance, 2D MHEM also present higher thermal stability (**Figure 8d–f**), making them ideal candidates for applications in harsh conditions. For instance, as a catalyst for reverse water gas shift reaction (RWGS), 2D high-entropy Cu₂Zn₁Al_{0.5}Ce₅Zr_{0.5}O_x retains the morphological structure even at 800 °C.^[66] In contrast, nanoparticle sintering was observed in the Cu₂Ce₇O_x catalyst during the heating process at lower temperatures, suggesting poor thermostability. Thus, the structural stability of 2D MHEMs can be exploited for catalytic reactions under harsh conditions.

4.4. Versatile Electromagnetic Properties

The unique structural versatility and chemical diversity of 2D MHEMs offer a flexible platform for discovering unconventional physical and chemical phenomena. For instance, Hideo et al.

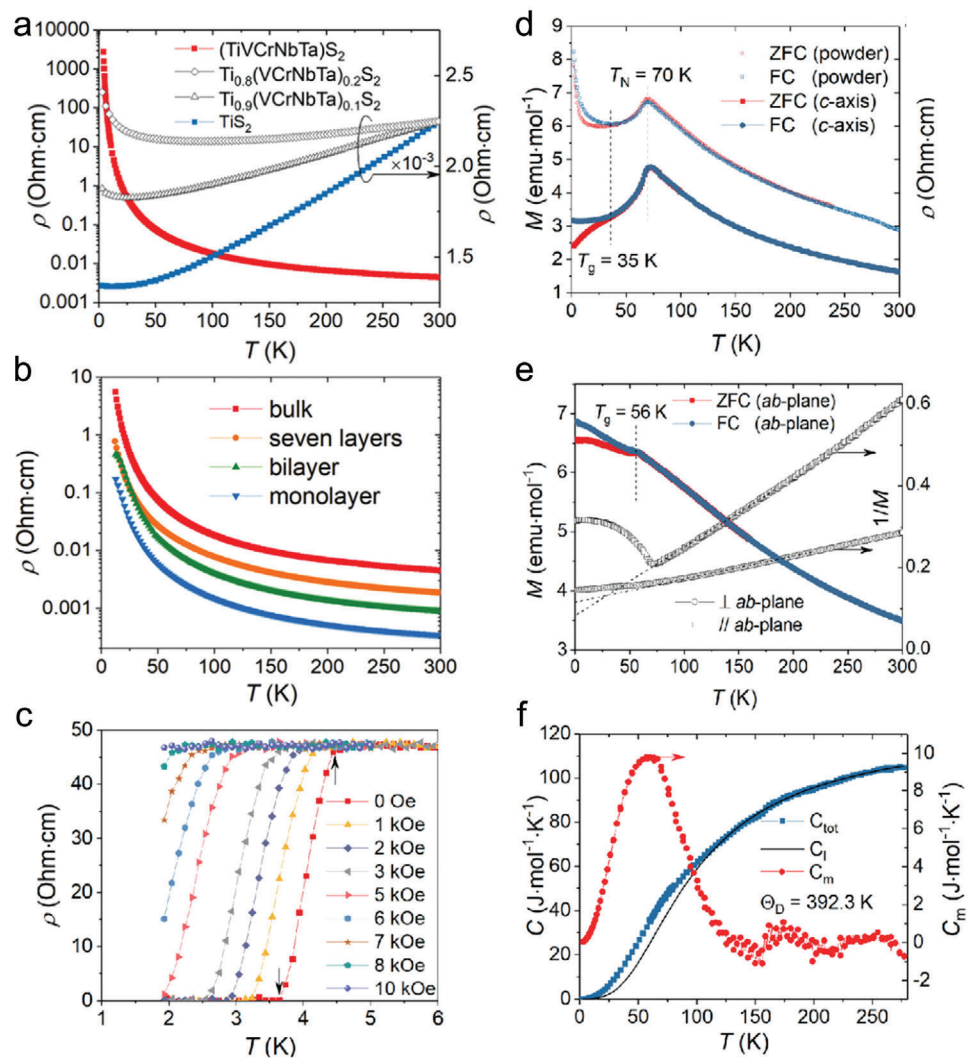


Figure 9. Unique properties of 2D MHEMs, including electrical and magnetic properties. a) Resistivity curves. The Metal-insulator transition was influenced by composition in high-entropy $(\text{TiVCrNbTa})\text{S}_2$. b) Resistivity of high-entropy $(\text{TiVCrNbTa})\text{S}_2$ at different thickness from 12 to 300 K. c) Superconductivity of high-entropy $(\text{Co, Au})_{0.2}(\text{Rh, Ir, Pt, Pd})_{0.8}\text{Te}_2$. d, e) The magnetization tests of $(\text{Mn, Fe, Co, Ni})\text{PS}_3$, which were conducted under the external magnetic field $H = 500$ Oe vertical to or parallel the ab-plane. f) Heat capacity of $(\text{Mn, Fe, Co, Ni})\text{PS}_3$ from 2 to 280 K. Reproduced with permission.^[18] Copyright 2021, American Chemical Society.

systematically investigated the physical characteristics, including electrical and magnetic properties of high-entropy vdW materials (Figure 9), and their relationship with chemical tunability.^[18] As shown in Figure 9a, a metal-insulator transition phenomenon was observed between $(\text{TiVCrNbTa})\text{S}_2$ and original TiS_2 due to high entropy effects. Furthermore, in contrast to the electrical behavior of conventional bulk TMC, the resistivity of high-entropy $(\text{TiVCrNbTa})\text{S}_2$ witnessed a decrease upon thickness reduction (Figure 9b). Surprisingly, superconductivity was also observed in high-entropy $(\text{Co, Au})_{0.2}(\text{Rh, Ir, Pt, Pd})_{0.8}\text{Te}_2$, which might be ascribed to the formation of Te-Te dimer (Figure 9c). The magnetic properties of high-entropy vdW materials were also explored. For instance, pristine mono-metal phosphorus trichalcogenides (i.e., $(\text{Mn, Fe, Co, Ni})\text{PS}_3$) exhibit characteristic behaviors of Heisenberg magnets and anisotropic Heisenberg magnets in MnPS_3 and NiPS_3 , respectively. As shown in

Figure 9d, $(\text{Mn, Fe, Co, Ni})\text{PS}_3$ presents an antiferromagnetic transition behavior at 70 K under an external magnetic field along the *c*-axis. As the temperature dropped, a spin glass transition was also observed at 35 K. Once setting an external magnetic field along the ab-plane direction, spin glass transition appeared at 56 K (Figure 9e). The heat capacity test further confirmed the Heisenberg-type antiferromagnetic transition (Figure 9f). So far, the research on electrical and magnetic properties of 2D MHEM is still at a preliminary stage. Therefore, considering the complexity of 2D MHEM structure and composition, further efforts are needed to find the influencing factors such as atomic radius, electronegativity, chemical bond length, lattice distortion, and thickness. High-throughput computation might be a useful tool to predict the structure-to-properties relationship by constructing accurate atomic distribution and electronic structure.

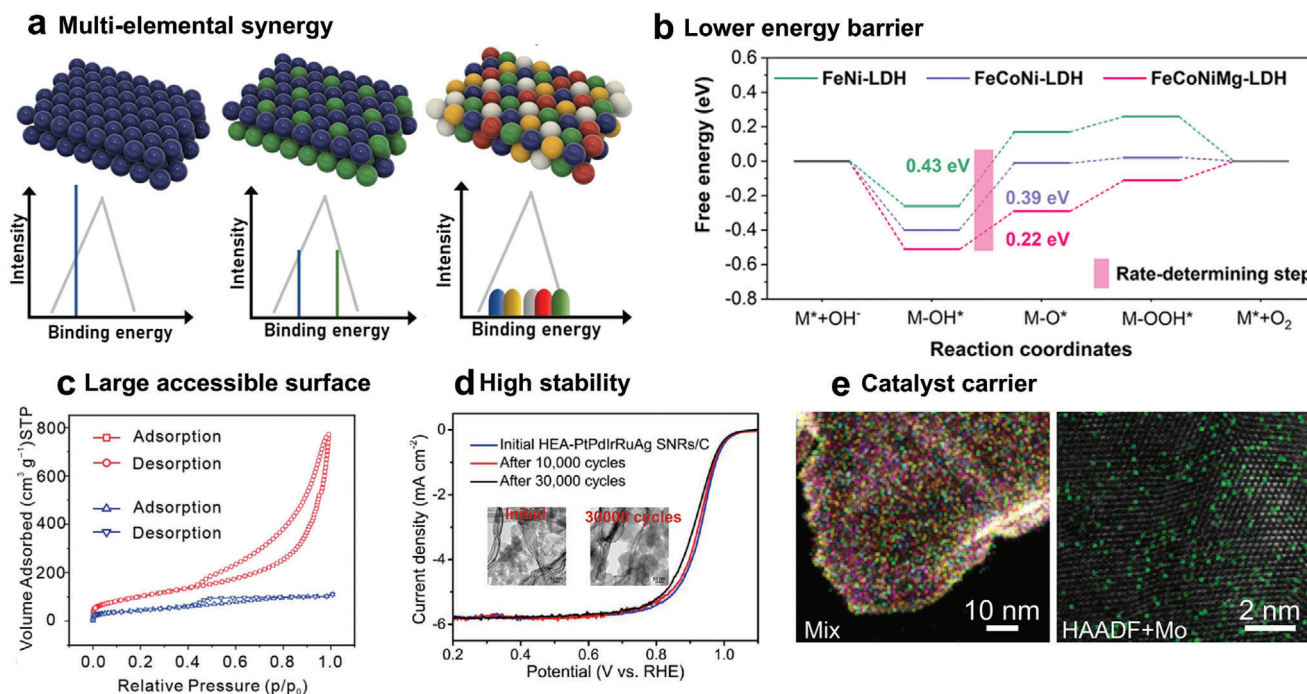


Figure 10. a) The multi-elemental synergy mechanism of high-entropy MHEMs. The diverse element types, concentration, and unordered distribution of MHEMs contribute to continuous surface binding energy. Reproduced with permission.^[70] Copyright 2021, Wiley-VCH. b) The variations comparison of Gibbs free energy in the four-step OER process. It is apparent that FeCoNiMg-LDH delivers more favorable catalysis kinetics. Reproduced with permission.^[71] Copyright 2023, American Chemical Society. c) N₂ adsorption and desorption curves of MOFs derived monolayer high-entropy hydroxalates (red) and amorphous hydroxalates obtained by the alkali coprecipitation method (blue). The calculated specific surface area is 380.5 and 164.2 mg²/g. Reproduced with permission.^[52] Copyright 2023, Wiley-VCH. d) Linear sweep voltammograms and corresponding TEM images of high-entropy PtPdIrRuAg alloy nanoribbons during cycling. Reproduced with permission.^[38] Copyright 2022, American Chemical Society. e) Mo single atoms dispersed in 2D high-entropy PdPtNiCuZn alloys. Reproduced under the terms of the CC-BY-NC licence.^[78] Copyright 2024, Springer Nature.

5. 2D MHEMs Applications

5.1. Catalysis

The development of clean, renewable, and affordable energy technologies can reduce the extensive use of fossil fuels, which is crucial for the global transition to a greener, more sustainable future. Considering the highly abundant presence in nature, carbon dioxide and water serve as potential sources for generating efficient energy carriers like hydrogen, methanol, and ethanol.^[67] This objective can be achieved through techniques like photocatalysis, thermocatalysis, and electrocatalysis, including chemical reactions such as hydrogen evolution reaction (HER), oxygen evolution reaction, oxygen reduction reaction (ORR), carbon dioxide reduction reaction (CO₂RR), and others.^[68] To date, the majority of catalysts are composed of precious metals such as palladium, platinum, and ruthenium, thus they are impractical for industrial-scale production due to their scarcity and high cost.^[69] As a result, the development of high-performance catalysts through the substitution of precious metals with high-abundance elements is highly sought after.

2D MHEMs, in view of their high chemical tunability, multi-metal sites, and large surface area, are potential alternative catalysts. Table 2 summarizes the catalytic performances of representative 2D MHEMs and corresponding counterparts. Obviously, 2D MHEMs show excellent catalytic activity and high

stability in a variety of catalytic reactions, superior to low-entropy or bulk forms. In contrast to the discrete nature of binding energies in traditional materials, 2D MHEMs with unordered element distribution present uniform and wideband binding energies, which is the key to superior performance (Figure 10a).^[70] Thus, the excellent catalytic performance does not only arise from the elemental nature of MHEMs, but also from the synergistic induced effects, namely cocktail effects, which play a dominant role. Considering the high tunability in element types and concentrations, there are ample opportunities to integrate diverse active sites to optimize binding energy and achieve enhanced catalytic performances. Furthermore, the synergistic working effects can be evaluated by computational chemical methods. For example, in the four-step OER pathway under alkaline conditions, the electronic structure and variations of Gibbs free energy can be estimated by density functional theory calculations. As shown in Figure 10b, FeCoNiMg-LDH displays a lower energy barrier than FeNi-LDH and FeCoNi-LDH in the rate-determining step.^[71] The high-entropy coordination of FeCoNiMg-LDH generates synergistic electronic interactions that activate nickel (Ni) in spin-polarized states, elevating the Fermi level. This, in turn, optimizes the adsorption energy of intermediates and speeds up the kinetics of the oxygen evolution reaction (OER). Besides, the synthesis of FeCoNiMg-LDH, which incorporates elevated configuration entropy and reduced Gibbs free energy, coupled with the formation of Mg–O interfacial bonds, ensures a stable crystal

Table 2. Catalytic performance of representative 2D MHEMs.

HER	Electrolyte	Overpotential [mV]	Tafel slope [mV dec ⁻¹]	Stability	Ref
PdMoGaInNi alloy	0.5 M H ₂ SO ₄	13	149	12 h no decay	[73]
Pd		42	185.1	Unstable	
Co _{0.6} (VMnNiZn) _{0.4} PS ₃	1 M KOH	65.9	65.5	12 h small loss	[43]
CoPS ₃		202.8	93.5	~	
PdPtRhIrCu	1 M KOH	15	37	20 h small loss	[79]
Pd		273	173	~	
(MoWReMnCr) ₂ S ₂	0.5 M H ₂ SO ₄	127	111.6	20 h small loss	[55]
MoS ₂		219	133.8	~	
OER	Electrolyte	Overpotential [mV]	Tafel slope [mV dec ⁻¹]	Stability	
LiMoFeCoNi-LDH	1 M KOH	187	82	12 h no decay	[46]
FeNi-LDH		232	112	~	
M-RuIrFeCoNiO ₂	0.5 M H ₂ SO ₄	189	49	120 h no decay	[44]
M-RuO ₂		210	51	10 h large loss	
FeCoMoWO _x	1 M KOH	332	63.6	self-healing	[65]
FeCoO _x		365	63.2	self-healing	
(NiFeCoMn) ₃ S ₄	1 M KOH	289	75.6	1000 cycles no decay	[80]
(NiFe) ₃ S ₄		413	101.6	~	
GaFeCoNiMo	1 M KOH	240	37.9	250 h small loss	[63]
GaFeCoNi		383	60.6	~	
ZnCoNiFeV-LDH	1 M KOH	253	49	1000 h small loss	[52]
NiCo-LDH		347	~	~	
FeCoNiMg-LDH	1 M KOH	302	75	60 h small loss	[71]
FeNi-LDH		347	83	60 h large loss	
Au _{5A} -MnFeCoNiCuLDH	1 M KOH	213	27.5	700 h small loss	[42]
MnFeCoNiCuLDH		323	85.5	~	
ORR	Electrolyte	Half-wave potential [V]	Mass activity [A mg noble metal ⁻¹]	Stability	
PtPdIrRuAg alloy	0.1 M KOH	0.93	4.28	10 000 cycles	[38]
Pt/C		0.85	0.2	Unstable	
CoFeNiMnCuZnO _x -PMA	0.1 M KOH	0.802 under light	~	~	[81]
NiMnCuZnO _x -PMA		~0.700 under light	~	~	
Pt ₃₂ Pd ₄₈ Ni ₂₀	0.1 M KOH	0.89	0.54	10 000 cycles no decay	[37]
Pd/C		0.82	0.07	~	
CO ₂ RR	Electrolyte	Current (A cm ⁻²)	Potential (V)	Stability	
(MoWNbTaV) ₂ S ₂	1 M KOH and 1 M choline chloride	0.51	-0.8	20 h small loss	[75]
RWGS	Feed gas	CO production rate (mmol g ⁻¹ h ⁻¹)	Selectivity	Stability	
Cu ₂ Zn ₁ Al _{0.5} Ce ₅ Zr _{0.5} O _x	CO ₂ /H ₂ = 1/1 with 40 sccm flow rate	417.2	100%	stable	[66]
Cu ₂ Ce ₇ O _x		~50	~	unstable	

structure and mitigates phase segregation, enabling exceptional stability and long-term catalytic performance.

Considering that most of the catalytic reactions occur at interfaces, the surface structure of the catalyst is key. In general, nanoscale electrocatalysts deliver enhanced catalytic properties than bulk counterparts due to the greater amount of exposed metal sites.^[72] In this case, the atomic-thickness effects endow MHEMs with a large accessible surface area. For instance, MOF-derived monolayer high-entropy hydroxalicates exhibit a large specific surface area of $380.5 \text{ m}^2 \text{ g}^{-1}$, which promotes the catalytic efficiency (Figure 10c).^[52] In addition, another key point worth mentioning is the sluggish diffusion effects of 2D MHEMs. Several studies have demonstrated that the sluggish diffusion effects slow down the phase transition and stabilize the microstructure of MHEMs, which contributes to high stability in catalytic reactions.^[73–76] As shown in Figure 10d, even after 30 000 cycles, high-entropy PtPdIrRuAg alloy nanoribbons still remain similar catalytic performance and morphologic structure in ORR.^[38] Especially, the high durability of 2D MHEMs greatly increases their potential in harsh environments. For instance, in seawater electrolysis, the catalyst must endure oxidation and reduction induced by the electric field, as well as withstand corrosion from seawater.^[77] Despite this, the loss of catalytic activity is still inevitable in long-term work under harsh conditions. So, this raises the question: Can the activity of the catalyst be regenerated? In a recent work by Kang et al., self-healing of catalytic activity was discovered in 2D high-entropy oxides.^[65] After 100 h cycling in borate buffer (KBi, pH = 14) containing Co^{2+} electrolyte solution, the FeCoNiWO_x catalyst shows reduce of overpotential and Tafel slope. However, the underlying mechanism of self-healing still needs further investigation. In situ characterizations during electrocatalytic reactions might enhance the understanding of the evolution of catalyst structures during self-healing. Recently, 2D MHEMs have also been used as catalyst carriers to design high-performance compound catalysts. The atomic-thickness effect endures ample surface area for loading various highly active atoms.^[42,78] For instance, single-atom Mo was shown to be deposited in 2D high-entropy PdPtNiCuZn alloys to catalytic methanol oxidation reactions. This offers a novel approach to designing high-performance catalysts, namely the precise structural integration of 2D MHEMs with other high-activity components (Figure 10e).

5.2. Energy Storage

Developing renewable and clean energy sources to replace the burning of fossil fuels, such as wind, tidal, and solar energy, is instrumental in tackling the escalating environmental issues and global climate changes.^[82–84] Electrochemical energy storage technology, as a key supporting technology for the energy revolution, plays a decisive role in advancing society. To date, much attention has been paid to the development of various electrochemical energy storage devices, including supercapacitors, lithium-ion batteries (LIB), potassium-ion batteries (PIB), lithium metal batteries (LMB), and lithium-sulfur batteries.^[85–87] Despite the progress, electrochemical energy storage devices still rely on conventional architectures based on cathode, anode, electrolyte, and separator, respectively.^[88] Thus, it is expected that

high-performance devices can be achieved through the utilization of advanced materials in the construction of these components.

Among various electrochemical energy devices, supercapacitors and LIB attracted the most attention. Supercapacitors offer the advantages of high-power density ($>1000 \text{ W kg}^{-1}$) and stable cycling life (over 10 000 cycles), but they suffer from low energy density ($<10 \text{ Wh/kg}$).^[89] On the contrary, LIB presents favorable energy density, but ordinary power density and stability. In this case, the 2D MHEMs with high chemical tunability are the potential option to solve these fundamental challenges. Table 3 reviews the energy storage performances of representative 2D MHEMs. Generally, there are two main electrochemical mechanisms for both supercapacitors and batteries: capacitive contribution related to the surface structure and faradaic pseudocapacitance contribution involved with elements' redox properties.^[90] Compared to conventional materials, 2D MHEMs electrodes feature superior capacity, favorable rate capability, and long cycling life, which is ascribed to its core effects. First, the atomic thickness of 2D MHEMs guarantees optimal interface, through enhanced contact, with the surface of the electrode and the electrolyte, which is the basis of an efficient charge transfer between electrolyte and electrode. Moreover, the ultimate thinness extended the application of MHEMs to flexible energy storage devices. As shown in Figure 11a, 2D high-entropy $\text{Ti}_{1.1}\text{V}_{0.7}\text{Cr}_x\text{Nb}_{1.0}\text{Ta}_{0.6}\text{C}_3\text{T}_z$ is easily integrated into a flexible membrane electrode via vacuum filtration.^[40] Second, the strong lattice distortion of 2D MHEMs improves the kinetics of redox reactions at the electrode/electrolyte interface, leading to increased capacity. Last, 2D MHEMs show high durability being key to suppressing the occurrence of side reactions during cycling. In this context, Yang et al. showed that high mechanical strain induced by lattice distortion could effectively promote the Li nucleation and growth uniformly on the high-entropy $(\text{TiVZrNbTa})_2\text{CT}_x$ surface (Figure 11b), resolving the dendritic crystal issue.^[64] Furthermore, stable stripping and plating of Li can last up to 500 h in a galvanostatic cycling test, indicating favorable stability. Due to their chemical and structural versatility, 2D MHEMs can also be employed as electrolytes and separators. As shown in Figure 11c, Yang et al. discovered that 2D high-entropy $\text{Li}_x(\text{Fe}_{1/5}\text{Co}_{1/5}\text{Ni}_{1/5}\text{Mn}_{1/5}\text{Zn}_{1/5})\text{PS}_3$ serves as an excellent Li^+ conductor, boasting high conductivity up to $5 \times 10^{-4} \text{ S cm}^{-1}$.^[91] To verify the practical application capability, $\text{Li}_x(\text{Fe}_{1/5}\text{Co}_{1/5}\text{Ni}_{1/5}\text{Mn}_{1/5}\text{Zn}_{1/5})\text{PS}_3$ was integrated with nitrile-butadiene rubber to construct a solid-state electrolyte for lithium metal batteries. Similarly, 2D MHEMs can also be assembled into a separator to catalytic the S conversion in Li-S batteries (Figure 11d).^[92] The in situ Raman spectrums reveal that $\text{LaFe}_{0.4}\text{Co}_{0.2}\text{Ni}_{0.2}\text{Cu}_{0.2}\text{O}_3$ based separator suppresses the precipitation of lithium sulfides, which contributes to a high capacity and stable cycling life. Overall, the core effects of 2D MHEMs have shown considerable impacts on electrochemical performances yet their potential in advanced energy storage applications is still uncharted.

5.3. Electronic Applications

The extended compositional and structural tunability of 2D MHEMs can be further exploited to broaden the range of

Table 3. Energy storage performance of representative 2D MHEMs.

Supercapacitors	Capacity [F/g]	Rate capability	Stability	Ref
Ti ₂ V _{0.9} Cr _{0.1} C ₂ T _x	553.3	good	small loss after 2000 cycles	[41]
Ti ₃ C ₂ T _x	~350	bad	~	
Ti _{1.1} V _{0.7} Cr _x Nb _{1.0} Ta _{0.6} C ₃ T _z	490	good	89% retention after 9000 cycles	[40]
LIB	Capacity [mAh/g]	Rate capability	Stability	
(TiVNbTaMo) ₂ C	283	good	300 cycles no decay	[93]
(TiVNbTa) ₂ C	276	bad	300 cycles no decay	
(TiVNb) ₂ C	276	moderate	300 cycles no decay	
(CoCuMgNiZn)O	450	good	200 cycles no decay	[47]
PIB	Capacity [mAh/g]	Rate capability	Stability	
(CoMnFeZn)PS ₃	524	good	1000 cycles no change	[94]
(CoMnFe)PS ₃	≈520	moderate	400 cycles large loss	
FePS ₃	≈480	bad	200 cycles large loss	
LMB solid electrolyte	Li ⁺ conductivity [S cm ⁻¹]	Coulombic efficiency	Stability	
Li _x (Fe _{1/5} Co _{1/5} Ni _{1/5} Mn _{1/5} Zn _{1/5})PS ₃	5 × 10 ⁻⁴	99.8%	800 h small loss	[91]
Li _x FePS ₃	≈1 × 10 ⁻⁶	~	~	
LMB	Li nucleation overpotential [mV]	Rate capability	Stability	
(TiVZrNbTa) ₂ CT _x	6	good	small loss after 1200 h	[64]
Ti ₂ C ₂ T _x	34	bad	large loss after 500 h	
Li-S separator	Catalyze sulfur conversion	Capacity [mAh/g]	Stability	
(TiVZrNbTa) ₂ C _x N _{1-x} T _y	efficient	702	small loss after 360 cycles	[95]
Ti ₂ C _{1/2} N _{1/2} T _x	inefficient	~	~	
TiVNbMoC ₃	efficient	948.5	1200 cycles no decay	[96]
Ti ₄ C ₃	inefficient	~	~	
LaFe _{0.4} Co _{0.2} Ni _{0.2} Cu _{0.2} O ₃	efficient	1199.8	0.041% decay per cycle	[92]
SERS	Bandgap [eV]	Detection limit [R6G]	Stability	
MnFeCuAgInPS ₃	0.43	10 ⁻⁹ M	6 months, workable in acid/alkaline conditions	[97]
MnPS ₃	2.35	Bad	~	

applicability, to include electronic devices application.^[98–100] As the progress in electronics is still at an early stage, understanding how entropy engineering can alter the electronic/magnetic/thermal properties represents a core issue.^[101] For instance, the strong lattice distortion in semiconducting 2D MHEMs induces a series of structural defects, such as vacancies and grain boundaries, which directly affect the carrier migration, making the design of 2D MMHEs with tailored semiconducting characteristics represent a major challenge. Nevertheless, preliminary studies in the development of semiconductive 2D MHEMs by tuning their composition to modulate the band structure have been carried out.^[102] As shown in **Figure 12a**, the spectral and Mott–Schottky characterizations revealed that entropy engineering of 2D MnPS₃ effectively changes valence and conduction band, thus acquiring high-entropy MnNiCuInSnPS₃ with 0.43 eV bandgap.^[97] To gain insight into the influence of each element on band structure, DFT calculations were performed on an optimized crystal structure model. The substantial continuous *d*-electron states of Mn, Fe, and Cu play a predominant role in filling and narrowing the bandgap instead of the *p*-electron states of P and S atoms (**Figure 12a**). This facilitates the occupation of

energies near the Fermi level and increases the density of states, which suggests the regulation of electronic structure from component modulation. To explore practical applications, 2D high-entropy MnNiCuInSnPS₃ was employed in surface-enhanced Raman scattering, exhibiting a low detection limit with 10⁻⁹ M for rhodamine 6G.

2D MHEMs also show potential in other electronics applications. Entropy engineering has been demonstrated to promote the enhanced capacitive energy storage of dielectrics.^[103] In the latest work, an entropy-stabilized dielectric film based on Bi₂Ti₂O₇ was reported and boasting an impressive energy density of 182 J cm⁻³ with an efficiency of 78% at 6.35 MV cm⁻¹. In-depth studies indicate that favorable and stable microscopic structural characteristics are introduced upon modulation of the atomic configuration entropy, including lattice-distorted nanocrystals and disordered quasi-amorphous phases, which deliver enhanced disruptive strength, energy storage density, and efficiency. Moreover, entropy engineering was also adopted to improve the piezoelectric and thermoelectric performance of transition metal chalcogenide.^[104] For example, a piezoelectric coefficient of 4.22 pm V⁻¹ was achieved

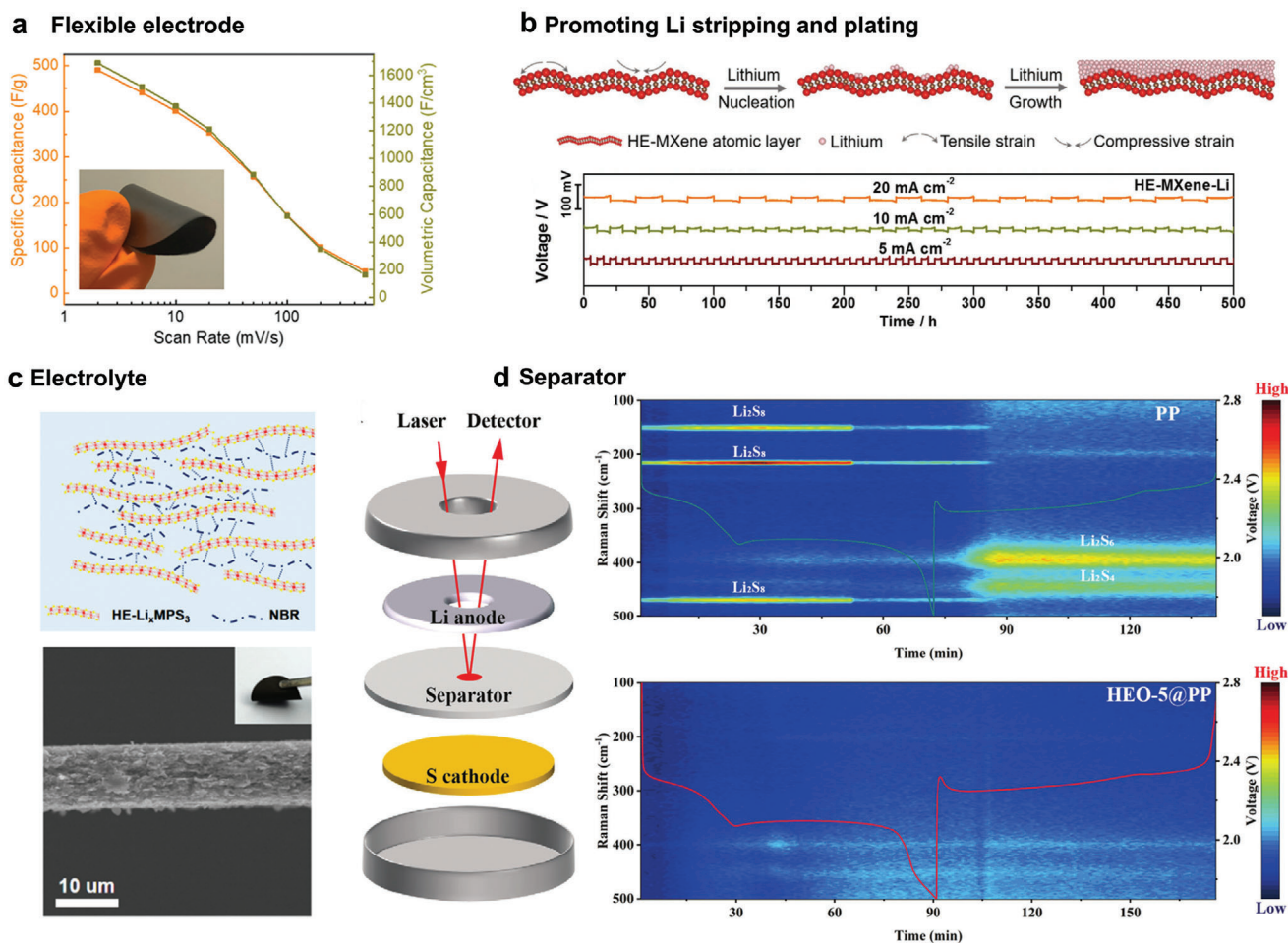


Figure 11. Energy storage applications of 2D MHEMs. a) 2D high-entropy $\text{Ti}_{1.1}\text{V}_{0.7}\text{Cr}_x\text{Nb}_{1.0}\text{Ta}_{0.6}\text{C}_3\text{T}_z$ as flexible electrode for supercapacitors. Obviously, MXene is easily integrated into flexible membrane electrodes via vacuum filtration. Reproduced with permission.^[40] Copyright 2022, American Chemical Society. b) Li stripping and plating on $(\text{TiVZrNbTa})_2\text{CT}_x$ surface. 2D $(\text{TiVZrNbTa})_2\text{CT}_x$ is stable in 500 h galvanostatic cycling. Reproduced with permission.^[64] Copyright 2021, Wiley-VCH. c) 2D high-entropy $\text{Li}_x(\text{Fe}_{1/5}\text{Co}_{1/5}\text{Ni}_{1/5}\text{Mn}_{1/5}\text{Zn}_{1/5})\text{PS}_3$ with high Li^+ conductivity was applied to build solid-state electrolytes in lithium metal batteries. Reproduced with permission.^[91] Copyright 2023, American Chemical Society. d) 2D high-entropy $\text{LaFe}_{0.4}\text{Co}_{0.2}\text{Ni}_{0.2}\text{Cu}_{0.2}\text{O}_3$ was applied to construct the Li-S batteries separator. In situ Raman spectrums prove the suppression effect of $\text{LaFe}_{0.4}\text{Co}_{0.2}\text{Ni}_{0.2}\text{Cu}_{0.2}\text{O}_3$ on lithium sulfide precipitation. Reproduced with permission.^[92] Copyright 2024, Wiley-VCH.

in 2D medium-entropy $\text{Mo}_{0.46}\text{W}_{0.54}\text{S}_2$, much higher than that of bare MoS_2 and WS_2 (Figure 12c). Overall, the electronic applications of 2D MHEMs are still in the early stages, and more effects are needed to reveal the relationship between the core effects of MHEMs and electronic/magnetic/thermal properties.

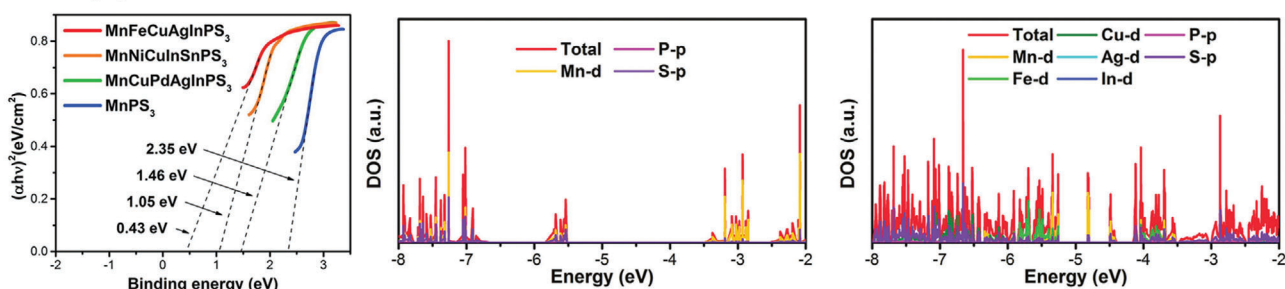
Understanding the structure-to-activity relationship in 2D MHEMs is critical to exploit their full potential. 2D MHEMs present core effects, including entropy, lattice distortion, sluggish diffusion, cocktail, and atomic thickness, as shown in Figure 13. In addition, some MHEMs exhibit further characteristic behaviors that differ from mono- and bi-elemental 2D systems. First, 2D MHEMs show more accessible and larger active surfaces than conventional materials, enhancing the catalytic performance. Second, due to the diversity of atoms involved, pronounced lattice distortion of 2D MHEMs induces strong mechanical strain, enabling unusual curved nanosheet morphology, inducing the increase of active surface and endowing deformability function.

Third, 2D MHEMs present abundant defects, lattice distortions, grain boundaries, and unsaturated sites, changing the intrinsic electronic structure and chemical activity. For instance, enhanced electrocatalytic activity and sluggish dynamics in energy storage devices were observed because of the crystal defects and vacancies.

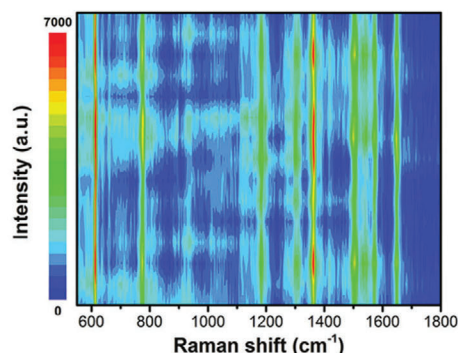
6. Summary and Outlook

The combination of entropy engineering and atomic thickness has delivered a vast and versatile library of 2D materials with enticing physicochemical properties. So far, a series of 2D MHEMs have been designed and produced, such as MXene, oxides, TMC, LDH, and alloys. Thus, to gain insights into this emerging class of materials, we critically assessed their synthesis, structure, properties, and applications. (Figure 13) First, state-of-the-art synthetic techniques, including wet-chemical doping, CVD doping, and atomic exchange alloying were discussed, bringing

a Bandgap Variations



b SERS



c Piezoelectric Electronics

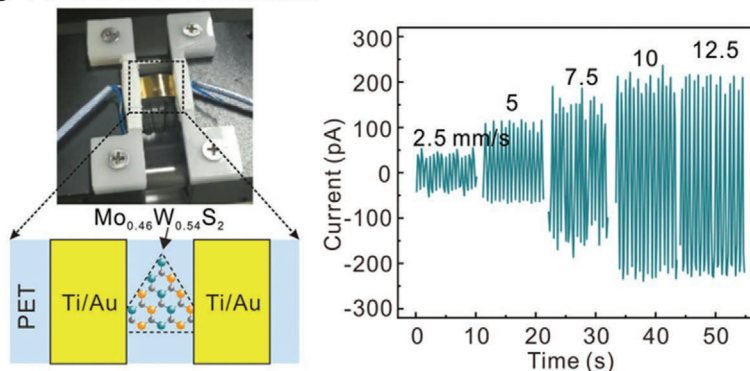


Figure 12. a) Bandgap variations induced by entropy engineering toward transition-metal phosphorus sulfides. The band gap spectra of MnPS_3 , MnCuPdAgInPS_3 , MnFeCuAgInPS_3 and MnNiCuInSnPS_3 are presented. Density functional theory calculations were performed and the density of the state of $\text{Mn}_8\text{P}_8\text{S}_{24}$ (MnPS_3 model) and $\text{Mn}_2\text{Fe}_2\text{Cu}_2\text{Ag}_1\text{In}_1\text{P}_8\text{S}_{24}$ (MnNiCuInSnPS_3 model) are displayed. b) SERS performance of rhodamine 6G (10^{-6} M) on MnNiCuInSnPS_3 . Reproduced with permission.^[97] Copyright 2024, Wiley-VCH. c) Piezoelectric application of 2D medium-entropy $\text{Mo}_{0.46}\text{W}_{0.54}\text{S}_2$. Reproduced with permission.^[104] Copyright 2022, Wiley-VCH.

forward the need for further efforts toward the achievement of phase control in 2D MHEMs. Second, structural defects (i.e., vacancies, dislocations, unsaturated sites, and grain boundaries) and atomically distributed lattice strains arising from the lattice distortion induced by the 2D confinement were reviewed, as they strongly affect the thermal, electrical, and magnetic properties of 2D MHEMs and thus, their applications. In particular,

the core effects of 2D MHEMs, such as cocktail, sluggish-diffusion, atomic-thickness, and drastic-lattice-distortion, play critical roles in the device performance of specific applications ranging from catalysis to (opto)electronics and energy storage. Despite of great progress achieved thus far, some key points require more attention for the future endeavor in this research direction.

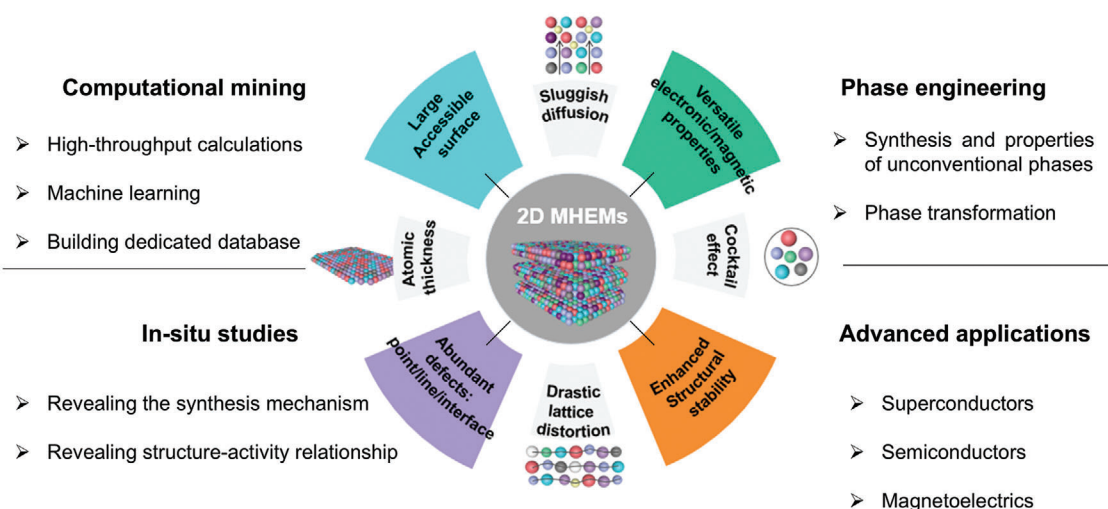


Figure 13. Schematic depiction of the core effects, properties, and future developments of 2D MHEMs.

6.1. Computational Mining

To date, the experimental approaches driven by trial-and-error strategies limit the advancement of 2D MHEMs. In contrast, due to the structural complexity and diversity of this class of materials, the integration of computational strategies could be instrumental in boosting the exploration and prediction of novel architectures. High-throughput calculations and machine learning can be exploited as powerful strategies to predict the fundamental properties of uncharted 2D MHEMs. For example, the calculated phase diagram method (CALPHAD) has been employed to identify the mechanical properties of high-entropy alloys.^[105] Nevertheless, the structural complexity as well as the uncertainty of atomic arrangement call for high computational power. Current calculations mainly focus on the thermodynamic equilibrium system of the bulk materials and have not yet been expanded to the 2D regime. Additionally, existing materials databases, such as *Computational 2D Materials Database (C2DB)*, *Materials Cloud*, and *Materials Project*, contain limited examples of MHEMs that are clearly described or labeled, failing to offer enough statistics for machine training algorithms. Therefore, establishing a dedicated database for such materials would foster their development.

6.2. Phase Engineering

The structural phase shaped by the arrangement and organization of atoms within the lattice is crucial to impart 2D MHEMs programmed mechanical, thermal, and electrical properties. However, the precise control over the structural phase of 2D MHEMs represents still a challenge. Indeed, phase engineering in MHEMs is hampered by the endless combination of the elemental composition induced by extreme synthesis conditions in the state-of-the-art approaches. Thus, developing growth techniques with atomic precision would represent a step forward toward phase control of these architectures. Currently, 2D MHEMs are restricted to a reduced amount of phase structures, such as MXene, hydroalcites, and alloy with Face Center Cubic (FCC) structure. Other forms including 2D nitrides and phosphide are still unexplored as efficient synthetic methodologies are still missing. Designing multiphase 2D MHEMs-based composites or heterostructures, especially unconventional crystal phases, represents an avenue holding great promise in fundamental science and practical applications, as new physicochemical properties of 2D MHEMs can be uncovered.

6.3. In Situ Studies

Further efforts are required to unveil the structure versus property relationship in such a wide family of materials. Advanced characterizations have played a pivotal role in thoroughly assessing the complex chemical composition of 2D MHEMs. So far, the phase, morphology, and elemental composition of 2D MHEMs have been explored by advanced structural characterizations like diffraction (X-ray and neutron diffraction), microscopy (AFM, SEM, TEM, STEM), and spectroscopy (XPS, XANES, EXAFS) techniques. To retrieve correlations between synthesis and fundamental structural information of 2D MHEMs, in situ characteri-

zations need further exploration. First, in situ and *operando* characterizations can monitor the synthetic reaction process cast light onto key parameters of the growth mechanism, and target the design of MHEMs with desired structures. For example, a high-temperature alloying reaction was mimicked in *operando* environmental TEM, which enabled the monitoring of the fusion-splitting-fission-crystallization growth process in high-entropy alloy nanoparticles on liquid Ga.^[62] Moreover, in situ and *operando* characterizations can be exploited to provide further insights into the structural evolution of MHEMs using on-chip electronic devices under operational conditions. For instance, the lattice distortion evolution of 2D MHEMs during the catalytic process, as well as the intercalation and de-intercalation of ions occurring in the 2D MHEMs lattice in batteries, can be elucidated. Therefore, dynamic structural characterizations are of paramount importance in unraveling the structure versus properties relationship of 2D MHEMs, ultimately boosting their technological relevance.

6.4. Advanced Applications

The large compositional and structural diversity of 2D MHEMs provides a versatile platform for a wide range of applications. The majority of reported works have delivered successful proof-of-concept devices in the field of electrocatalysis (i.e., HER, OER, ORR, and CO₂RR) and energy storage (i.e., supercapacitors and batteries). To further extend the scope of reach, combinatorial synthesis, controlling the elemental composition of 2D MHEMs, can be used to replace conventional toxic or noble metals as catalysts, achieving high catalytic activity and stability at reduced costs and detrimental environmental impact. In addition, 2D MHEMs represent a valuable alternative as electrode materials for solving the capacity loss caused by surface reconstruction and phase transition during the rapid charge-discharge process or long-term cycles occurring in energy storage devices. Also, enhanced stability can be achieved through compositional engineering, providing stable electrode materials for applications under extreme conditions, such as high temperature and high pressure. To push forward the development of such a versatile class of emerging materials, the 2D design and entropic engineering, leading to the control over the phase and electronic structure, will enable the exploration of multifunctional devices in the fields of optoelectronics, photonics, sensing, and beyond.

Ultimately, the 2D MHEMs are key components with chemically programmable and enhanced functional complexity that can be exploited in future disruptive high performance applications in catalysis, energy storage, and electronics, thereby becoming gamechangers for addressing global challenges.

Acknowledgements

The authors gratefully acknowledge the financial support from the National Natural Science Foundation of China (grant nos. 22205141 and 22209051), the Shanghai Pujiang Program, China (grant no. 22PJ1408300), and the Fundamental Research Funds for the Central Universities of China (grant no. 23 × 010301599, 24 × 010301678). Further, The authors gratefully acknowledge financial support from the European Commission through the ERC project SUPRA2DMAT (GA-833707) and the HORIZON-CL4-2023-DIGITAL-EMERGING-01-CNECT

project 2D-PRINTABLE (GA-101135196) as well as the Agence Nationale de la Recherche through the Interdisciplinary Thematic Institute SysChem via the IdEx Unistra (ANR-10-IDEX-0002) within the program Investissement d'Avenir and the Foundation Jean-Marie Lehn.

Conflict of Interest

The authors declare no conflict of interest.

Keywords

2D materials, entropy engineering, high-entropy materials, medium-entropy materials

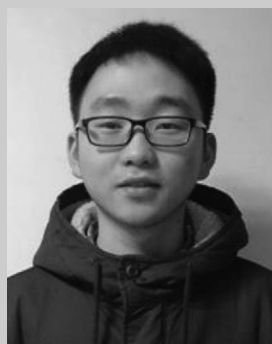
Received: August 23, 2024

Revised: October 11, 2024

Published online: October 28, 2024

- [1] Y. Ding, C. Wang, M. Zeng, L. Fu, *Adv. Mater.* **2023**, 35, 2306689.
- [2] J. W. Yeh, S. K. Chen, S. J. Lin, J. Y. Gan, T. S. Chin, T. T. Shun, C. H. Tsau, S. Y. Chang, *Adv. Eng. Mater.* **2004**, 6, 299.
- [3] R. Liu, H. Chen, K. Zhao, Y. Qin, B. Jiang, T. Zhang, G. Sha, X. Shi, C. Uher, W. Zhang, L. Chen, *Adv. Mater.* **2017**, 29, 1702712.
- [4] W. Li, D. Xie, D. Li, Y. Zhang, Y. Gao, P. K. Liaw, *Prog. Mater. Sci.* **2021**, 118, 100777.
- [5] Y. F. Ye, Q. Wang, J. Lu, C. T. Liu, Y. Yang, *Mater. Today* **2016**, 19, 349.
- [6] Y. Ma, Y. Ma, Q. Wang, S. Schweidler, M. Botros, T. Fu, H. Hahn, T. Brezesinski, B. Breitung, *Energy Environ. Sci.* **2021**, 14, 2295.
- [7] E. P. George, D. Raabe, R. O. Ritchie, *Nat. Rev. Mater.* **2019**, 4, 515.
- [8] L. Sun, R. J. Cava, *Phys. Rev. Mater.* **2019**, 3, 90301.
- [9] G. Feng, F. Ning, Y. Pan, T. Chen, J. Song, Y. Wang, R. Zou, D. Su, D. Xia, *J. Am. Chem. Soc.* **2023**, 145, 11140.
- [10] S. Akrami, P. Edalati, M. Fuji, K. Edalati, *Mat. Sci. Eng. R.* **2021**, 146, 100644.
- [11] Y. Yao, Q. Dong, A. Brozena, J. Luo, J. Miao, M. Chi, C. Wang, I. G. Kevrekidis, Z. J. Ren, J. Greeley, G. Wang, A. Anapolsky, L. Hu, *Science* **2022**, 376, eabn3103.
- [12] S. Schweidler, M. Botros, F. Strauss, Q. Wang, Y. Ma, L. Velasco, G. Cadilha Marques, A. Sarkar, C. Kübel, H. Hahn, J. Aghassi-Hagmann, T. Brezesinski, B. Breitung, *Nat. Rev. Mater.* **2024**, 9, 266.
- [13] C. Tan, X. Cao, X. Wu, Q. He, J. Yang, X. Zhang, J. Chen, W. Zhao, S. Han, G. Nam, M. Sindoro, H. Zhang, *Chem. Rev.* **2017**, 117, 6225.
- [14] A. Gupta, T. Sakthivel, S. Seal, *Prog. Mater. Sci.* **2015**, 73, 44.
- [15] Y. Sun, W. Wu, L. Yu, S. Xu, Y. Zhang, L. Yu, B. Xia, S. Ding, M. Li, L. Jiang, J. Duan, J. Zhu, S. Chen, *Carbon Energy* **2023**, 5, 1.
- [16] S. K. Nemani, B. Zhang, B. C. Wyatt, Z. D. Hood, S. Manna, R. Khaledialidusti, W. Hong, M. G. Sternberg, S. K. R. S. Sankaranarayanan, B. Anasori, *ACS Nano* **2021**, 15, 12815.
- [17] D. Zhang, H. Zhao, B. Huang, B. Li, H. Li, Y. Han, Z. Wang, X. Wu, Y. Pan, Y. Sun, X. Sun, J. Lai, L. Wang, *ACS Central Sci* **2019**, 5, 1991.
- [18] T. Ying, T. Yu, Y. Shiah, C. Li, J. Li, Y. Qi, H. Hosono, *J. Am. Chem. Soc.* **2021**, 143, 7042.
- [19] S. K. Nemani, M. Torkamanzadeh, B. C. Wyatt, V. Presser, B. Anasori, *Commun. Mater.* **2023**, 4, 16.
- [20] T. Ying, T. Yu, Y. Qi, X. Chen, H. Hosono, *Adv. Sci.* **2022**, 9, 2203219.
- [21] X. Han, G. Wu, S. Zhao, J. Guo, M. Yan, X. Hong, D. Wang, *Matter* **2023**, 6, 1717.
- [22] Y. Sun, S. Dai, *Sci. Adv.* **2021**, 7, eabg1600.
- [23] Y. Cui, Y. Zhang, Z. Cao, J. Gu, Z. Du, B. Li, S. Yang, *SusMat* **2022**, 2, 65.
- [24] S. S. Aamlid, M. Oudah, J. Rottler, A. M. Hallas, *J. Am. Chem. Soc.* **2023**, 145, 5991.
- [25] L. Liu, Y. Zhang, J. Han, X. Wang, W. Jiang, C. T. Liu, Z. Zhang, P. K. Liaw, *Adv. Sci.* **2021**, 8, 2100870.
- [26] D. B. Miracle, O. N. Senkov, *Acta Mater.* **2017**, 122, 448.
- [27] A. Sarkar, Q. Wang, A. Schiele, M. R. Chellali, S. S. Bhattacharya, D. Wang, T. Brezesinski, H. Hahn, L. Velasco, B. Breitung, *Adv. Mater.* **2019**, 31, 1806236.
- [28] B. Fultz, *Prog. Mater. Sci.* **2010**, 55, 247.
- [29] W. Hsu, C. Tsai, A. Yeh, J. Yeh, *Nat. Rev. Chem.* **2024**, 8, 471.
- [30] X. Wang, W. Guo, Y. Fu, *J. Mater. Chem. A* **2021**, 9, 663.
- [31] S. Yang, P. Zhang, A. S. Nia, X. Feng, *Adv. Mater.* **2020**, 32, 1907857.
- [32] S. Pinilla, J. Coelho, K. Li, J. Liu, V. Nicolosi, *Nat. Rev. Mater.* **2022**, 7, 717.
- [33] Z. Dai, L. Liu, Z. Zhang, *Adv. Mater.* **2019**, 31, 1805417.
- [34] S. Ranganathan, *Curr. Sci.* **2003**, 85, 1404.
- [35] J. T. Ren, L. Chen, H. Y. Wang, Z. Y. Yuan, *Chem. Soc. Rev.* **2023**, 52, 8319.
- [36] X. Xiao, L. Yang, W. Sun, Y. Chen, H. Yu, K. Li, B. Jia, L. Zhang, T. Ma, *Small* **2022**, 18, 2105830.
- [37] J. Lai, F. Lin, Y. Tang, P. Zhou, Y. Chao, Y. Zhang, S. Guo, *Adv. Energy Mater.* **2019**, 9, 1800684.
- [38] L. Tao, M. Sun, Y. Zhou, M. Luo, F. Lv, M. Li, Q. Zhang, L. Gu, B. Huang, S. Guo, *J. Am. Chem. Soc.* **2022**, 144, 10582.
- [39] T. Wang, Q. He, J. Zhang, Z. Ding, F. Li, Y. Yang, *Mater. Today* **2020**, 36, 30.
- [40] J. Zhou, Q. Tao, B. Ahmed, J. Palisaitis, I. Persson, J. Halim, M. W. Barsoum, P. O. Å. Persson, J. Rosen, *Chem. Mater.* **2022**, 34, 2098.
- [41] W. Ma, M. Wang, Q. Yi, D. Huang, J. Dang, Z. Lv, X. Lv, S. Zhang, *Nano Energy* **2022**, 96, 107129.
- [42] F. Wang, P. Zou, Y. Zhang, W. Pan, Y. Li, L. Liang, C. Chen, H. Liu, S. Zheng, *Nat. Commun.* **2023**, 14, 6019.
- [43] R. Wang, J. Huang, X. Zhang, J. Han, Z. Zhang, T. Gao, L. Xu, S. Liu, P. Xu, B. Song, *ACS Nano* **2022**, 16, 3593.
- [44] C. Hu, K. Yue, J. Han, X. Liu, L. Liu, Q. Liu, Q. Kong, C. Pao, Z. Hu, K. Suenaga, D. Su, Q. Zhang, X. Wang, Y. Tan, X. Huang, *Sci. Adv.* **2023**, 9, eadf9144.
- [45] Y. Yao, Z. Huang, P. Xie, S. D. Lacey, R. J. Jacob, H. Xie, F. Chen, A. Nie, T. Pu, M. Rehwoldt, D. Yu, M. R. Zachariah, C. Wang, R. Shahbazian-Yassar, J. Li, L. Hu, *Science* **2018**, 359, 1489.
- [46] X. Yu, B. Wang, C. Wang, C. Zhuang, Y. Yao, Z. Li, C. Wu, J. Feng, Z. Zou, *Small* **2021**, 17, 2103412.
- [47] J. Wei, K. Rong, X. Li, Y. Wang, Z. Qiao, Y. Fang, S. Dong, *Nano Res.* **2022**, 15, 2756.
- [48] J. Li, F. L. Deepak, *Chem. Rev.* **2022**, 122, 16911.
- [49] M. Kim, I. Oh, H. Choi, W. Jang, J. Song, C. S. Kim, J. Yoo, S. Cho, *Cell Rep. Phys. Sci.* **2022**, 3, 100702.
- [50] X. Zhao, Z. Xue, W. Chen, X. Bai, R. Shi, T. Mu, *J. Mater. Chem. A* **2019**, 7, 26238.
- [51] H. Mei, Y. Mei, S. Zhang, Z. Xiao, B. Xu, H. Zhang, L. Fan, Z. Huang, W. Kang, D. Sun, *Inorg. Chem.* **2018**, 57, 10953.
- [52] Y. Ding, Z. Wang, Z. Liang, X. Sun, Z. Sun, Y. Zhao, J. Liu, C. Wang, Z. Zeng, L. Fu, M. Zeng, L. Tang, *Adv. Mater.* **2023**, 2302860.
- [53] X. Chu, J. Li, W. Qian, H. Xu, *Chem. Rec.* **2023**, 23, e202200222.
- [54] L. Chen, Y. Li, K. Chen, X. Bai, M. Li, S. Du, Z. Chai, Q. Huang, *Small Struct.* **2023**, 4, 2200161.
- [55] J. Qu, A. Elgendy, R. Cai, M. A. Buckingham, A. A. Papaderakis, H. de Latour, K. Hazeldine, G. F. S. Whitehead, F. Alam, C. T. Smith, D. J. Binks, A. Walton, J. M. Skelton, R. A. W. Dryfe, S. J. Haigh, D. J. Lewis, *Adv. Sci.* **2023**, 10, 2204488.
- [56] Y. Wei, P. Zhang, R. A. Soomro, Q. Zhu, B. Xu, *Adv. Mater.* **2021**, 33, 2103148.

- [57] M. Li, X. Xi, H. Wang, X. Lyu, Z. Li, R. Zhu, X. Ren, D. Yang, A. Dong, *J. Colloid Interface Sci.* **2022**, 617, 500.
- [58] T. G. Ritter, A. H. Phakatkar, M. G. Rasul, M. T. Saray, L. V. Sorokina, T. Shokuhfar, J. M. Gonçalves, R. Shahbazian-Yassar, *Cell Rep. Phys. Sci.* **2022**, 3, 100847.
- [59] H. Xu, Z. Zhang, J. Liu, C. Do-Thanh, H. Chen, S. Xu, Q. Lin, Y. Jiao, J. Wang, Y. Wang, Y. Chen, S. Dai, *Nat. Commun.* **2020**, 11, 3908.
- [60] M. Hu, J. Liu, S. Song, W. Wang, J. Yao, Y. Gong, C. Li, H. Li, Y. Li, X. Yuan, Z. Fang, H. Xu, W. Song, Z. Li, *ACS Catal.* **2022**, 12, 3238.
- [61] N. Kar, M. McCoy, J. Wolfe, S. L. A. Bueno, I. H. Shafei, S. E. Skrabalak, *Nat. Synth.* **2024**, 3, 175.
- [62] G. Cao, J. Liang, Z. Guo, K. Yang, G. Wang, H. Wang, X. Wan, Z. Li, Y. Bai, Y. Zhang, J. Liu, Y. Feng, Z. Zheng, C. Lu, G. He, Z. Xiong, Z. Liu, S. Chen, Y. Guo, M. Zeng, J. Lin, L. Fu, *Nature* **2023**, 619, 73.
- [63] J. Liang, J. Liu, H. Wang, Z. Li, G. Cao, Z. Zeng, S. Liu, Y. Guo, M. Zeng, L. Fu, *J. Am. Chem. Soc.* **2024**, 146, 7118.
- [64] Z. Du, C. Wu, Y. Chen, Z. Cao, R. Hu, Y. Zhang, J. Gu, Y. Cui, H. Chen, Y. Shi, J. Shang, B. Li, S. Yang, *Adv. Mater.* **2021**, 33, 2101473.
- [65] D. Gao, W. Zhu, J. Chen, K. Qin, M. Ma, J. Shi, Q. Wang, Z. Fan, Q. Shao, F. Liao, M. Shao, Z. Kang, *ACS Catal.* **2024**, 14, 3700.
- [66] Y. Li, X. Bai, D. Yuan, C. Yu, X. San, Y. Guo, L. Zhang, J. Ye, *Nat. Commun.* **2023**, 14, 3171.
- [67] L. Tang, X. Meng, D. Deng, X. Bao, *Adv. Mater.* **2019**, 31, 1901996.
- [68] H. Li, J. Lai, Z. Li, L. Wang, *Adv. Funct. Mater.* **2021**, 31, 2106715.
- [69] J. Ren, L. Chen, H. Wang, Z. Yuan, *Chem. Soc. Rev.* **2023**, 52, 8319.
- [70] T. Löffler, A. Ludwig, J. Rossmeisl, W. Schuhmann, *Angew. Chem., Int. Ed.* **2021**, 133, 27098.
- [71] D. Liu, X. Yan, P. Guo, Y. Yang, Y. He, J. Liu, J. Chen, H. Pan, R. Wu, *ACS Catal.* **2023**, 13, 7698.
- [72] Y. Zhou, X. Shen, T. Qian, C. Yan, J. Lu, *Nano Res.* **2023**, 16, 7874.
- [73] X. Fu, J. Zhang, S. Zhan, F. Xia, C. Wang, D. Ma, Q. Yue, J. Wu, Y. Kang, *ACS Catal.* **2022**, 12, 11955.
- [74] D. Feng, Y. Dong, P. Nie, L. Zhang, Z. Qiao, *Chem. Eng. J.* **2022**, 430, 132883.
- [75] J. Cavin, A. Ahmadiparidari, L. Majidi, A. S. Thind, S. N. Misal, A. Prajapati, Z. Hemmat, S. Rastegar, A. Beukelman, M. R. Singh, K. A. Unocic, A. Salehi Khojin, R. Mishra, *Adv. Mater.* **2021**, 33, 2100347.
- [76] I. S. Kwon, S. J. Lee, J. Y. Kim, I. H. Kwak, G. M. Zewdie, S. J. Yoo, J. Kim, K. Lee, J. Park, H. S. Kang, *ACS Nano* **2023**, 17, 2968.
- [77] W. He, X. Li, C. Tang, S. Zhou, X. Lu, W. Li, X. Li, X. Zeng, P. Dong, Y. Zhang, Q. Zhang, *ACS Nano* **2023**, 17, 22227.
- [78] L. He, M. Li, L. Qiu, S. Geng, Y. Liu, F. Tian, M. Luo, H. Liu, Y. Yu, W. Yang, S. Guo, *Nat. Commun.* **2024**, 15, 2290.
- [79] Q. Mao, X. Mu, K. Deng, H. Yu, Z. Wang, Y. Xu, X. Li, L. Wang, H. Wang, *Adv. Funct. Mater.* **2023**, 33, 2304963.
- [80] L. Wu, X. Shen, Z. Ji, J. Yuan, S. Yang, G. Zhu, L. Chen, L. Kong, H. Zhou, *Adv. Funct. Mater.* **2023**, 33, 2208170.
- [81] H. Ge, L. Zheng, G. Yuan, W. Shi, J. Liu, Y. Zhang, X. Wang, *J. Am. Chem. Soc.* **2024**, 146, 10735.
- [82] J. Xiao, F. Shi, T. Glossmann, C. Burnett, Z. Liu, *Nat. Energy* **2023**, 8, 329.
- [83] F. Zhang, B. He, Y. Xin, T. Zhu, Y. Zhang, S. Wang, W. Li, Y. Yang, H. Tian, *Chem. Rev.* **2024**, 124, 4778.
- [84] A. Schneemann, R. Dong, F. Schwotzer, H. Zhong, I. Senkovska, X. Feng, S. Kaskel, *Chem. Sci.* **2021**, 12, 1600.
- [85] S. Yang, P. Zhang, F. Wang, A. G. Ricciardulli, M. R. Lohe, P. W. M. Blom, X. Feng, *Angew. Chem., Int. Ed.* **2018**, 57, 15491.
- [86] H. Jin, S. Xin, C. Chuang, W. Li, H. Wang, J. Zhu, H. Xie, T. Zhang, Y. Wan, Z. Qi, W. Yan, Y. R. Lu, T. S. Chan, X. Wu, J. B. Goodenough, H. Ji, X. Duan, *Science* **2020**, 370, 192.
- [87] Y. Pei, Q. Chen, M. Wang, P. Zhang, Q. Ren, J. Qin, P. Xiao, L. Song, Y. Chen, W. Yin, X. Tong, L. Zhen, P. Wang, C. Xu, *Nat. Commun.* **2022**, 13, 6158.
- [88] S. Ferrari, M. Falco, A. B. Muñoz García, M. Bonomo, S. Brutti, M. Pavone, C. Gerbaldi, *Adv. Energy Mater.* **2021**, 11, 2100785.
- [89] M. Gao, F. Wang, S. Yang, A. Gaetano Ricciardulli, F. Yu, J. Li, J. Sun, R. Wang, Y. Huang, P. Zhang, X. Lu, *Mater. Today* **2024**, 72, 318.
- [90] J. Liu, J. Wang, C. Xu, H. Jiang, C. Li, L. Zhang, J. Lin, Z. X. Shen, *Adv. Sci.* **2018**, 5, 1700322.
- [91] Q. Zhao, Z. Cao, X. Wang, H. Chen, Y. Shi, Z. Cheng, Y. Guo, B. Li, Y. Gong, Z. Du, S. Yang, *J. Am. Chem. Soc.* **2023**, 145, 21242.
- [92] B. Wang, J. Tang, S. Jia, Z. Xing, S. Chen, Y. Deng, X. Meng, S. Tang, *Adv. Funct. Mater.* **2024**, 34, 2315836.
- [93] L. Chen, Y. Li, K. Liang, K. Chen, M. Li, S. Du, Z. Chai, M. Naguib, Q. Huang, *Small Methods* **2023**, 7, 2300054.
- [94] P. Chien, C. Chang, H. Tuan, *Energy Storage Mater.* **2023**, 61, 102853.
- [95] Z. Du, C. Wu, Y. Chen, Q. Zhu, Y. Cui, H. Wang, Y. Zhang, X. Chen, J. Shang, B. Li, W. Chen, C. Liu, S. Yang, *Adv. Energy Mater.* **2022**, 12, 2103228.
- [96] Q. Liang, S. Wang, X. Lu, X. Jia, J. Yang, F. Liang, Q. Xie, C. Yang, J. Qian, H. Song, R. Chen, *ACS Nano* **2024**, 18, 2395.
- [97] R. Wang, M. Chen, J. Han, X. Zhang, Z. Zhang, T. Yao, Y. Wang, L. Xu, X. Wang, P. Xu, B. Song, *Adv. Funct. Mater.* **2024**, 34, 2312322.
- [98] Y. Zhang, L. Chen, H. Liu, S. Deng, H. Qi, J. Chen, *InfoMat* **2023**, 5, e12488.
- [99] M. Zhang, S. Lan, B. B. Yang, H. Pan, Y. Q. Liu, Q. H. Zhang, J. L. Qi, D. Chen, H. Su, D. Yi, Y. Y. Yang, R. Wei, H. D. Cai, H. J. Han, L. Gu, C. W. Nan, Y. H. Lin, *Science* **2024**, 384, 185.
- [100] H. Gao, K. Zhao, H. Wuliji, M. Zhu, B. Xu, H. Lin, L. Fei, H. Zhang, Z. Zhou, J. Lei, H. Chen, S. Wan, T. Wei, X. Shi, *Energy Environ. Sci.* **2023**, 16, 6046.
- [101] B. Jiang, Y. Yu, H. Chen, J. Cui, X. Liu, L. Xie, J. He, *Nat. Commun.* **2021**, 12, 3234.
- [102] S. Susarla, A. Kutana, J. A. Hachtel, V. Kochat, A. Apte, R. Vajtai, J. C. Idrobo, B. I. Yakobson, C. S. Tiwary, P. M. Ajayan, *Adv. Mater.* **2017**, 29, 1702457.
- [103] B. Yang, Y. Zhang, H. Pan, W. Si, Q. Zhang, Z. Shen, Y. Yu, S. Lan, F. Meng, Y. Liu, H. Huang, J. He, L. Gu, S. Zhang, L. Chen, J. Zhu, C. Nan, Y. Lin, *Nat. Mater.* **2022**, 21, 1074.
- [104] Y. Chen, Z. Tian, X. Wang, N. Ran, C. Wang, A. Cui, H. Lu, M. Zhang, Z. Xue, Y. Mei, P. K. Chu, J. Liu, Z. Hu, Z. Di, *Adv. Mater.* **2022**, 34, 2201630.
- [105] O. N. Senkov, J. D. Miller, D. B. Miracle, C. Woodward, *Nat. Commun.* **2015**, 6, 6529.



Hao Mei received his M.S. degree in chemistry from the China University of Petroleum (East China) in 2022. He is currently a Ph.D. candidate under the supervision of Prof. Sheng Yang at Frontiers Science Center for Transformative Molecules, Shanghai Jiao Tong University. His research work mainly focuses on the synthesis and application of 2D carbon-based materials.



Antonio Gaetano Ricciardulli received his Ph.D. degree in chemistry in 2018 at the Max Planck Institute for Polymer Research, Germany, working on solution-processed 2D materials for optoelectronics with Prof. Paul Blom. After, he had post-doctoral experiences in the groups of Prof. Michael Saliba and Prof. Paolo Samorì, at TU Darmstadt and Institut de Science et d'Ingénierie Supramoléculaires (ISIS), respectively. Since 2023, he is assistant professor at ISIS at the University of Strasbourg. Current research interests include the synthesis of functional 2D materials and heterostructures with tunable electronic characteristics, their application in multifunctional (opto)electronics and sensing, as well as device physics.



Paolo Samorì is distinguished professor at the University of Strasbourg and director of the Institut de Science et d'Ingénierie Supramoléculaires. He is Fellow of the Royal Society of Chemistry (FRSC), Fellow of the European Academy of Sciences (EURASC), Member of the Academia Europaea, Member of the German National Academy of Science and Engineering (ACATECH), Member of the Académie des Technologies and Foreign Member of the Royal Flemish Academy of Belgium for Science and the Arts (KVAB). His research interests comprise nanochemistry, supramolecular sciences, materials chemistry with specific focus on graphene and other 2D materials, functional organic/polymeric and hybrid nanomaterials for application in optoelectronics, energy, and sensing.



Sheng Yang received his Ph.D. degree in chemistry in 2018 at the Max Planck Institute for Polymer Research, Mainz, Germany, working on the electrochemical synthesis of 2D materials under the supervision of Prof. Xinliang Feng and Prof. Klaus Müllen. He worked as a postdoctoral scientist in the group of Prof. Jurgen H. Smet and Prof. Klaus von Klitzing at Max Planck Institute for Solid State Research (2018-2022). Currently, he is an associate professor at Frontiers Science Center for Transformative Molecules, Shanghai Jiao Tong University. His main research interests focus on the advanced synthesis of 2D materials and their applications in energy and electronic devices.